Influence of Initial Microstructure and Heating Rate on Kinetics of Phase Transformation in Medium Carbon Low Alloy Steel

by

Navneeth Rajakrishnan

THESIS PRESENTED TO ÉCOLE DE TECHNOLOGIE SUPÉRIEURE IN PARTIAL FULFILLMENT OF THE REQUIREMENTS FORTHE DEGREE OF DOCTOR OF PHILOSOPHY
Ph.D.

MONTREAL, < 4 JUNE 2026>

ÉCOLE DE TECHNOLOGIE SUPÉRIEURE
UNIVERSITÉ DU QUÉBEC

BOARD OF EXAMINERS

THIS THESIS HAS BEEN EVALUATED

BY THE FOLLOWING BOARD OF EXAMINERS

Mr. Mohammad Jahazi, Thesis Supervisor
Department of Mechanical Engineering, École de Technologie Supérieure

Mr. Henri Champliaud Thesis Co-supervisor
Department of Mechanical Engineering, École de Technologie Supérieure

Mr. Pinaki Bhattacharjee Thesis Co-supervisor
Department of Material Science and Metallurgical Engineering, Indian Institute of Technology, Hyderabad

Mr. Kim Khoa Nguyen, President of the Board of Examiners
Department of Electrical Engineering, École de Technologie Supérieure

Ms. Elmira Moosavi, Member of the jury
Department of Mechanical Engineering, École de Technologie Supérieure

Ms. Olga Palazhchenko, External Evaluator
Department of Chemical Engineering, University of New Brunswick

THIS THESIS WAS PRESENTED AND DEFENDED

IN THE PRESENCE OF A BOARD OF EXAMINERS AND PUBLIC

<24 APRIL 2026>

AT ÉCOLE DE TECHNOLOGIE SUPÉRIEUR

ACKNOWLEDGEMENTS

This doctoral journey would not have been possible without the extraordinary guidance and support from many individuals. I extend my deepest gratitude to my Thesis Supervisor, Prof. Mohammad Jahazi, and my Co-supervisors, Prof. Henri Champliaud and Prof. Pinaki Bhattacharjee, for their insightful mentorship, invaluable technical expertise, and belief in this project. Their academic rigor and consistent encouragement were the driving forces behind this work.

I am sincerely thankful to everyone who contributed to the technical execution of this research. A special thanks goes to Dr. Mohammad Saadati, Mr. Radu Romanica, and Dr. Alireza Khodabande for their dedicated assistance with the multiple laboratory work. I am also deeply appreciative of Dr. Morteza Sadeghifar for his essential support in refining the mathematical models and data analysis.

Finally, I owe a profound debt of thanks to my wife, Dhanya, for her endless patience, motivation, and understanding. My gratitude also extends to my parents, Rajakrishnan and Aruna, and all my cherished relatives who prayed and provided moral support as well-wishers. Their unconditional love and sacrifice provided the bedrock of support throughout my academic career.

INFLUENCE DE LA MICROSTRUCTURE INITIALE ET DE LA VITESSE DE CHAUFFAGE SUR LA CINÉTIQUE DE LA TRANSFORMATION DE PHASE DANS LES ACIERS À MOYEN CARBONE FAIBLEMENT ALLIÉS

NAVNEETH RAJAKRISHNAN

RÉSUMÉ

Cette thèse examine l'influence de la microstructure initiale et de la vitesse de chauffage sur la cinétique de formation de l'austénite dans les aciers faiblement alliés à teneur moyenne en carbone. Cette classe d'aciers représente une catégorie de matériaux essentiels pour diverses applications industrielles telles que les trains d'atterrissage des avions et les turbines hydrauliques. Comprendre et contrôler avec précision ces transformations de phase est primordial pour optimiser le traitement thermique, obtenir les microstructures désirées et prédire les propriétés mécaniques. Malgré leur importance, une compréhension complète de la cinétique de formation de l'austénite à partir de microstructures initiales de bainite et de martensite, en particulier l'interaction entre la taille de grain d'austénite antérieure (TGAA) et la vitesse de chauffage, représente un défi de recherche important.

La recherche comble cette lacune en employant une méthodologie multi-facette. La dilatométrie haute résolution a été utilisée pour des expériences de chauffage continu afin de quantifier la cinétique de transformation et les températures critiques. Des essais de trempe intermittente, associés à des techniques de caractérisations microstructurales avancées comprenant la microscopie optique, la microscopie électronique à balayage (MEB) et la diffraction des électrons rétrodiffusés (EBSD), ont été réalisés pour élucider les mécanismes sous-jacents de germination et de croissance de l'austénite. De plus, l'étude a développé et optimisé des modèles mathématiques, basés sur les théories de germination et de croissance contrôlées par la diffusion et affinés à l'aide d'un algorithme génétique, pour décrire avec précision les comportements cinétiques observés.

Les résultats révèlent que pour une microstructure initiale de martensite, l'affinage du grain, en particulier une réduction de la TGAA de 330 μm à 117 μm, accélère significativement le taux de formation de l'austénite sans modifier la température critique de formation de l'austénite (A_{c1}). La germination de l'austénite dans ces échantillons martensitiques se produit principalement aux joints de grains d'austénite antérieure. En ayant étandu l'investigation à une microstructure initiale de bainite, une distinction claire des températures critiques et de la cinétique de transformation a été observée, la bainite présentant une cinétique nettement plus lente que la martensite. L'impact de la vitesse de chauffage s'est avéré plus prononcé sur la bainite que sur la martensite, et les différences de taux de croissance entre les deux microstructures initiales sont attribuées à des variations dans la distribution du carbone au sein de leurs matrices respectives.

Ce travail a permis de développer et de valider avec succès des modèles mathématiques capables de prédire le degré de formation de l'austénite en fonction du temps, de la vitesse de

chauffage et de la microstructure initiale (martensite et bainite), fournissant ainsi des informations précieuses pour le contrôle précis du traitement thermomécanique dans ces d'acier critiques.

Mots-clés : Transformation de phase, Cinétique, Martensite, Bainite, Taille de grain d'austénite antérieure, Modèle mathématique.

INFLUENCE OF INITIAL MICROSTRUCTURE AND HEATING RATE ON KINETICS OF PHASE TRANSFORMATION IN MEDIUM CARBON LOW ALLOY STEEL

NAVNEETH RAJAKRISHNAN

ABSTRACT

This thesis investigates the critical influence of initial microstructure and heating rate on the kinetics of austenite formation in medium carbon low alloy steels, which are vital materials for various industrial applications such as landing gear and hydraulic turbines. Understanding and precisely controlling these phase transformations are paramount for optimizing thermal processing, achieving desired microstructures, and predicting mechanical properties. Despite their significance, a comprehensive understanding of the kinetics of austenite formation from initial bainite and martensite microstructures, particularly how prior austenite grain size (PAGS) and heating rate interact, presents a significant research challenge.

The research addresses this gap by employing a multi-faceted methodology. High-resolution dilatometry was utilized for continuous heating experiments to quantify transformation kinetics and critical temperatures. Intermittent quenching tests, coupled with advanced microstructural characterization techniques including optical microscopy, scanning electron microscopy (SEM), and electron backscatter diffraction (EBSD), were performed to elucidate the underlying nucleation and growth mechanisms of austenite. Furthermore, the study developed and optimized mathematical models, rooted in diffusion-controlled nucleation and growth theories and refined using a genetic algorithm, to accurately describe the observed kinetic behaviors.

The findings reveal that for an initial martensite microstructure, grain refinement, specifically a reduction in PAGS from 330 μm to 117 μm, significantly accelerates the rate of austenite formation without altering the critical austenite formation temperature (A_{c1}). Nucleation of austenite in these martensitic samples predominantly occurs at prior austenite grain boundaries. Extending the investigation to an initial bainite microstructure, a clear distinction in critical temperatures and transformation kinetics was observed, with bainite exhibiting slower kinetics compared to martensite. The impact of heating rate was found to be more pronounced on bainite than on martensite, and differences in growth rates between the two initial microstructures are attributed to varying carbon distributions within their respective matrices. This work successfully developed and validated mathematical models capable of predicting the extent of austenite formation as a function of time, heating rate, and initial microstructure (martensite and bainite), providing valuable insights for the precise control of thermomechanical processing in these critical steel alloys.

Keywords: Phase transformation, Kinetics, Martensite, Bainite, Prior austenite grain size, Mathematical model

TABLE OF CONTENTS

Page

LIST OF TABLES

Page

LIST OF FIGURES

LIST OF ABBREVIATIONS AND ACRONYMS

A_{c1}	Austenite start temperature / critical austenite formation temperature
A_{c3}	Austenite finish temperature
APT	Atom Probe Tomography
B	Bainite
BCC	Body-Centered Cubic
BCT	Body-Centered Tetragonal
CLTE	Coefficient of Linear Thermal Expansion
CTE	Coefficient of Thermal Expansion
EBSD	Electron Backscatter Diffraction
FCC	Face-Centered Cubic
GA	Genetic Algorithm
IQ	Image Quality
JMAK	Johnson-Mehl-Avrami-Kolmogorov
KAM	Kernel Average Misorientation
LG	Larger Grain Sizes
LST	Least Squares Technique
LVDT	Linear Variable Differential Transducer
M	Martensite
P	Pearlite
PAGBs	Prior Austenite Grain Boundaries
PAGS	Prior Austenite Grain Size

PNTT	Pearlite-to-Austenite Transition Temperature
Q&T	Quenching and Tempering
RA	Retained Austenite
SEM	Scanning Electron Microscopy
SG	Smaller Grain Sizes
TEM	Transmission Electron Microscopy
TRIP	Transformation-Induced Plasticity

LIST OF SYMBOLS AND UNITS OF MEASUREMENT

Symbol	Description	Associated Unit
A	Coefficient of activated growth site (grain boundary face)	Dimensionless
B	Coefficient of activated growth site (grain boundary edge)	Dimensionless
C	Coefficient of activated growth site (grain boundary corner)	Dimensionless
D	Prior Austenite Grain Size (PAGS) / Dimension of assumed cubic ferrite grain	μm
G	Rate of grain growth	m/s
ΔG	Thermodynamic driving force	J
ΔG_{act}	Gibbs energy for the activated transfer of atoms (activation energy)	J/atom
$\Delta G_{\alpha \rightarrow \gamma}$	Gibbs energy difference per atom between martensite and austenite phases	J/atom
ΔH	Enthalpy of activation per atom	J/atom
ΔS	Entropy of activation per atom	J/atom
ΔT	Change in temperature	K
$\dot{T}$	Heating rate	K/s
I	Nucleation rate (classic nucleation theory)	S^{-1}
k	Boltzmann constant	J/K
K_1	Temperature-dependent constant (Avrami equation)	Dimensionless
K_s, K_e, K_c	Coefficients for growth sites (surface, edge, corner)	Dimensionless

Symbol	Description	Associated Unit
L	Length	m
L_0	Initial sample length	m
L_v, S_v, C_v	Edge length, boundary area, and grain corner number per unit volume	m/m^3 (Edge), m^2/m^3 (Area), m^{-3} (Corner)
n	Kinetic exponent (JMAK equation)	Dimensionless
N	Nucleation rate	$m^{-3}\ S^{-1}$
Q_n, Q_g	Activation energies for nucleation and growth	J
R	Gas constant	J/(mol.K)
t	Time	s
T	Absolute temperature	K
t_p	Time for pearlite dissolution	s
$V\gamma$	Volume fraction of austenite	Dimensionless
V_p	Volume fraction of pearlite	Dimensionless
X	Transformed volume fraction (Avrami equation)	Dimensionless
α_L	Coefficient of linear thermal expansion (CLTE)	K^{-1}
δ	Boundary thickness	m
σ_0	Average inter-lamellar spacing of pearlite	m
ϑ	Frequency of atomic jump	s^{-1}

INTRODUCTION

Medium-carbon low-alloy steels are widely used in various industrial applications owing to their excellent combination of strength, toughness, and wear resistance. These steels typically contain 0.25-0.6% carbon and small amounts of alloying elements such as manganese, chromium, nickel, and molybdenum. Their versatility makes them ideal for manufacturing components, including gears, shafts, and structural parts, in the automotive, construction, and machinery industries. The mechanical properties of these steels can be tailored through heat-treatment processes, making them adaptable to diverse engineering requirements(Talebi, 2018).

Understanding the influence of the heating rate and initial microstructure on austenite formation kinetics is crucial for optimizing heat treatment processes and achieving the desired mechanical properties in medium-carbon low-alloy steels. The initial phase composition, prior austenite grain size, and heating rate significantly affect the nucleation and growth of austenite during the heating cycle. These factors determine the final austenite grain size, distribution, and homogeneity, which in turn influence the subsequent transformation products and the ultimate mechanical properties of the steel(Settimi et al., 2019). By comprehending these relationships, manufacturers can develop more efficient and effective heat-treatment strategies to enhance the performance and reliability of steel components.

Mathematical modeling of austenite formation kinetics in initial martensite and bainite microstructures plays a vital role in advancing our understanding of phase transformations in medium-carbon low-alloy steels. These models provide quantitative insights into the complex relationships among the heating rate, initial microstructure, and austenite formation, enabling more precise control over the final properties of the steel. By accurately predicting austenite formation under various heating conditions, mathematical models allow process optimization, reduced energy consumption, and improved product quality. These models contribute to the development of new alloy compositions and heat-treatment strategies, leading to more efficient and cost-effective manufacturing processes in the steel industry(Dannoshita et al., 2019).

Despite the significant progress in understanding these phase transformations, several existing challenges hinder a comprehensive and predictive approach to optimizing heat treatment processes. A primary challenge lies in the experimental difficulty of precisely monitoring and characterizing the rapid phase transformations that occur during heating. Techniques for in-situ observation at high temperatures are often complex, costly, and limited in their ability to capture the real-time evolution of microstructural changes. As a result, robust experimental data are scarce, under conditions of non-isothermal heating, which makes it challenging to validate mathematical models. This gap between theoretical prediction and experimental validation is a significant hurdle in the development of more accurate and reliable heat-treatment strategies.

Another major challenge is the inherent complexity of the multi-component systems and the interplay between different microstructural features. The kinetics of austenite formation are not only a function of the heating rate but are also influenced by the complexities of the microstructure and the complex morphology of the initial martensitic or bainitic phases. Existing models often rely on simplifying assumptions about these factors, which can limit their predictive accuracy, especially for a wide range of steel compositions or under novel heat-treatment conditions. There is a pressing need for more sophisticated models that can integrate the effects of multiple interacting variables and provide a holistic understanding of how these factors collectively govern the kinetics of austenite formation and the final mechanical properties of the steel.

The present thesis aims to address the above challenges and is divided into four chapters, as detailed below:

Chapter 1 begins with a section that reviews the existing literature that focuses on phase transformations in steel, their influencing factors, and mathematical models describing austenite formation kinetics. It covers fundamental concepts, the factors affecting

transformations, and various mathematical models. This review identifies research gaps and emphasizes the importance of ongoing studies on enhancing steel processing techniques.

Chapter 2 summarizes the materials examined and characterized in this study. It includes a description of each piece of equipment utilized and the experimental methods employed, providing a clearer depiction of the tests discussed in the subsequent chapters. Additionally, a review of the basics of dilatometry is included, as it is a crucial technique predominantly used in this project.

Chapter 3 investigates the impact of the prior austenite grain size (PAGS) on the kinetics of austenite formation in medium-carbon, low-alloy steel with an initial martensite microstructure. By examining two distinct PAGS values representative of industrial grain sizes, this study aimed to elucidate the relationship between grain refinement and austenite formation rates. Through high-resolution dilatometry, intermittent quenching tests, and advanced microscopy techniques, this study provides insight into the nucleation and growth mechanisms of austenite. The findings were further quantified and modeled using diffusion-controlled theories and genetic algorithm optimization, offering a valuable understanding of steel manufacturing processes and microstructure control.

Chapter 4 examines how the starting phase and heating rate affect the austenite formation kinetics, comparing initial martensite and bainite. This shows that the critical transformation temperatures vary between these phases, with the differences increasing at higher heating rates. Mathematical modelling describes the transformation kinetics of austenite formation, offering insights into the interplay between the microstructure, heating conditions, and austenite formation. These findings support improved heat-treatment strategies and steel-property optimization.

The conclusion will summarize the major findings and contributions of the work in relation to the established research objectives. The thesis will conclude with **Recommendations** for

future work, outlining promising directions for both fundamental and applied research to build upon the predictive framework established herein.

CHAPTER 1

LITERATURE REVIEW

1.1 Phase transformation overview

To provide a comprehensive overview of the phase transformation in medium-carbon low-alloy steel, it is imperative to introduce the iron-carbon phase diagram as shown in Figure 1.1. This diagram, which encompasses carbon concentrations of up to 6.7% (corresponding to the composition of cementite), delineates the equilibrium phases present at various temperatures. For steel, the pertinent section of the diagram focuses on the eutectoid point and a carbon content below 2.11%. At higher carbon concentrations, the material is classified as cast iron rather than steel.

Pure iron undergoes a significant crystallographic transformation when heated above 911.5 °C, transitioning from a body-centered cubic (BCC) structure to a face-centered cubic (FCC) structure. These structures correspond to the ferrite (α) and austenite (γ) phases, respectively. At temperatures exceeding 1396 °C but below the melting point of 1538 °C, a third phase, delta ferrite (δ) emerges, structurally like ferrite. The volumetric changes associated with these phase transitions are crucial for determining phase fractions through dilatometry.(Hunkel et al., 2018).

The addition of carbon alters the previously established temperature boundaries in the iron-carbon system. As carbon concentration increases from 0% to 0.77%, the austenite temperature range decreases, delineated by the A_3 boundary separating γ and γ+α regions. The eutectoid point, occurring at 727 °C, represents the lowest temperature for austenite formation. For carbon concentrations between 0.77% and 2.11%, the A_{CM} boundary separates γ and Fe_3C (cementite) phases. The A_1 boundary denotes the minimum temperature at which austenite can exist.

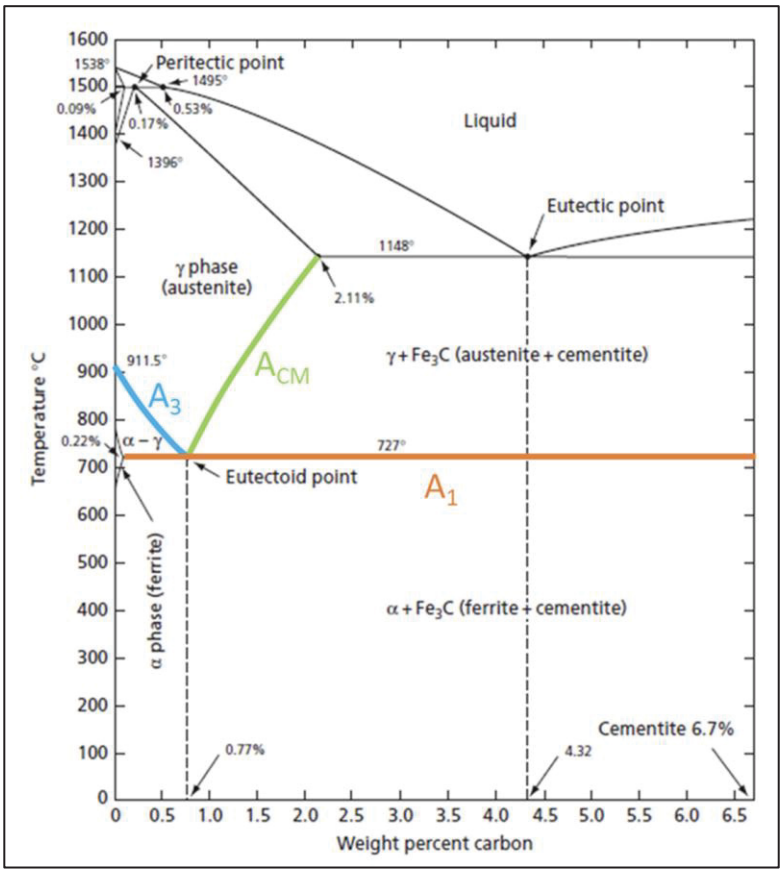

Figure 1.1 Iron-Carbon diagram
Taken fromChipman (1972)

While phase diagrams illustrate equilibrium conditions achieved through extremely slow cooling, practical heat treatment applications often involve non-equilibrium cooling rates. These accelerated cooling rates produce diverse microstructures, intentionally engineered to achieve specific mechanical properties. The formation of these microstructures can be categorized into two mechanisms: diffusive and displacive.

Diffusive or reconstructive transformation involves atomic rearrangement, resulting in a new crystal structure distinct from the parent phase. This process occurs at temperatures permitting sufficient atomic mobility, leading to compositional changes due to preferential element partitioning between parent and product phases(Porter et al., 2021).

Conversely, displacive or diffusionless transformation occurs through parent phase deformation without atomic diffusion. This process, known as invariant plane strain, involves shear deformation and dilatation. It typically occurs at lower temperatures, requiring high strain energy and a substantial driving force. The product phase maintains a composition like the parent phase due to the absence of atomic rearrangement (Eres-Castellanos et al., 2021).

1.1.1 Ferrite and pearlite

Ferrite and pearlite are two important phases in the iron-carbon system, playing crucial roles in determining the properties of steels and cast irons. These phases form at different temperatures and carbon concentrations, as illustrated in the iron-carbon phase diagram in Figure 1.2. Pearlite, on the other hand, is not a single phase but a lamellar structure consisting of alternating layers of ferrite and cementite (Fe_3C). It forms when austenite is cooled slowly through the eutectoid temperature (727 °C for plain carbon steels). The eutectoid composition occurs at approximately 0.76 wt% carbon, where austenite transforms entirely into pearlite. Pearlite exhibits a combination of strength and ductility, making it a desirable microstructure in many steel applications.

The formation and distribution of ferrite and pearlite in steel microstructures significantly influence the material's mechanical properties. By controlling the cooling rate and composition, metallurgists can manipulate the relative amounts and morphologies of these phases to achieve desired combinations of strength, ductility, and toughness in steel products(Callister & Rethwisch, 2018). Figure 1.3 shows a typical pearlitic microstructure.

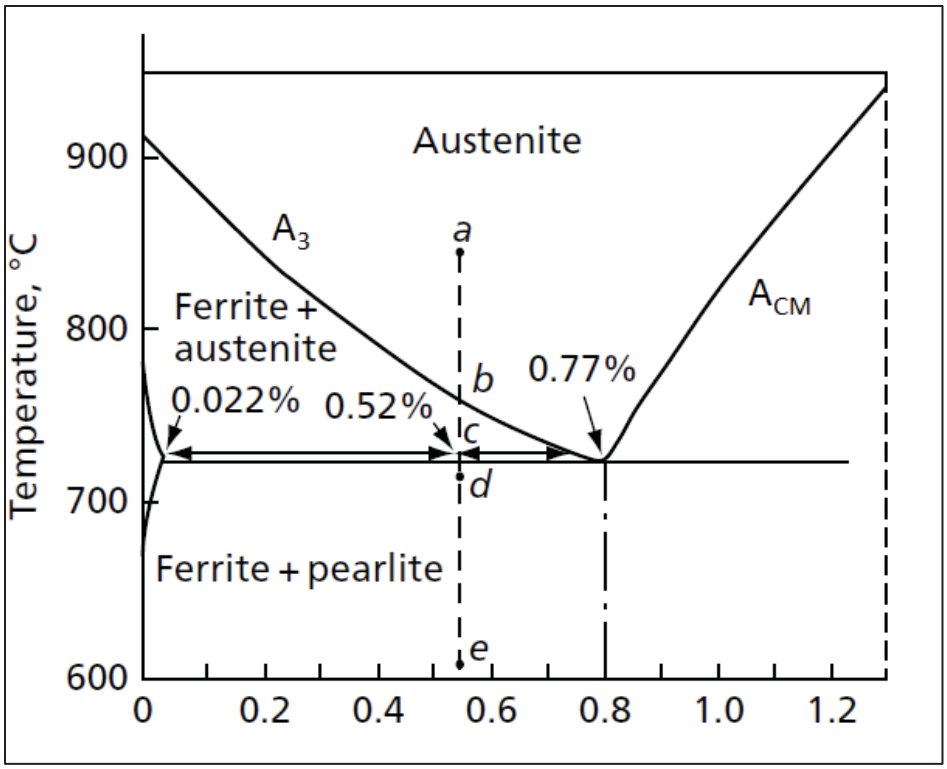

Figure 1.2 Transformation of a hypoeutectoid steel
Taken fromReed-Hill et al. (1973)

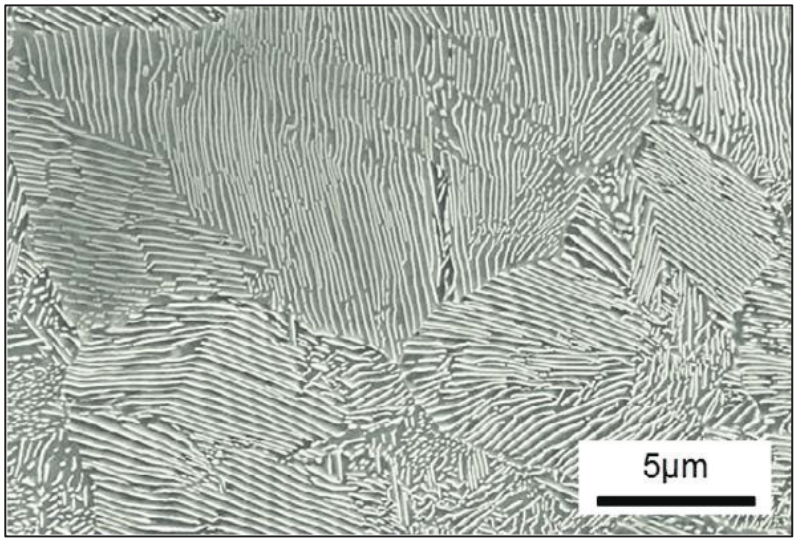

Figure 1.3 Microstructure of pearlite
Taken from Hamada et al. (2011)

1.1.2 Martensite

Martensite is a hard, metastable phase in steel that forms through a diffusionless transformation during rapid cooling, known as quenching. This phase is characterized by several key features that contribute to its unique properties and importance in steel metallurgy. The formation of martensite is classified as an athermal process because the transformation kinetics are not dependent on time (or thermal activation) but instead depend *almost solely* on the degree of supercooling below the equilibrium temperature. This means the transformation is driven by undercooling rather than time, which provides the necessary thermodynamic driving force (ΔG) to overcome the opposing strain energy and initiate the transformation. As a result, the reaction does not exhibit an incubation period or follow the time-dependent C-curves of diffusion-controlled reactions (like pearlite or bainite). Martensite forms nearly instantaneously as the material is cooled through the temperature range defined by the martensite start M_s and M_f temperatures. The total volume fraction of martensite formed is thus a direct function of the temperature achieved, as quantified by the Koistinen-Marburger relation, where cooling to a lower temperature immediately translates to a larger transformed volume(Bhadeshia, 2010). Structurally, this rapid, diffusionless shear process traps carbon atoms within the distorted lattice of the former face-centered cubic (FCC) austenite, resulting in the characteristic body-centered tetragonal (BCT) crystal structure (see Figure 1.4 for the BCT structure).

Due to the diffusionless nature of its formation, the composition of martensite remains similar to that of the parent austenite. This unique transformation process contributes to martensite's exceptional hardness, making it the hardest constituent among steel microstructures. However, this extreme hardness comes at the cost of poor ductility and a brittle nature, which can limit its applications in certain contexts. Martensite can manifest in two main morphological types: lath martensite, which forms in steels with carbon content below 0.6 wt. %, and plate martensite, which occurs in steels with carbon content between 0.6 and 1.8 wt. %. The degree of tetragonal distortion in the martensite structure is directly proportional to its carbon content, influencing its properties and behavior (Nishiyama, 2012).

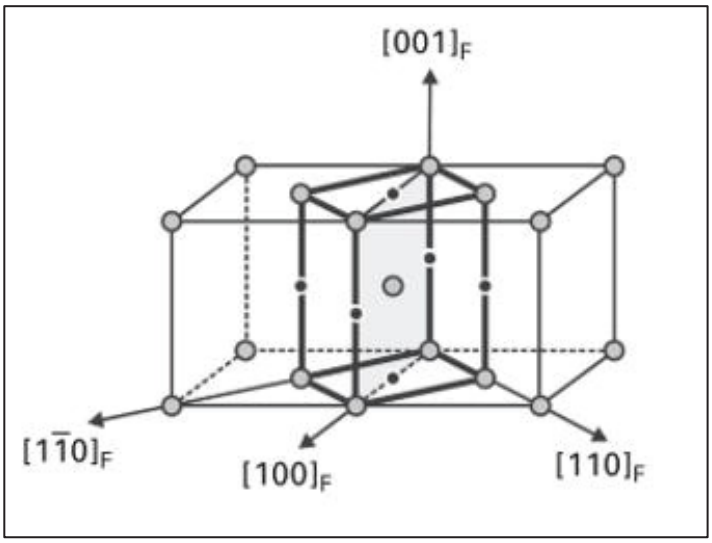

Figure 1.4 BCC structure of martensite shown within two FCC structure of austenite
Taken from Pereloma & Edmonds (2012)

1.1.3 Bainite

Bainite is a microstructure in steel that forms at temperatures between the pearlite and martensite transformation ranges. It was first identified by E.S. Davenport and E.C. Bain, who observed an “acicular, dark-etching aggregate”. Two distinct forms of bainite exist: upper bainite (400-550°C) and lower bainite (250-400°C) (Bhadeshia, 2019). Both consist of ferrite laths or plate aggregates called sheaves, with sub-units sharing a common crystallographic orientation. The primary distinction between upper and lower bainite lies in carbide distribution, as can be seen in Figure 1.5. In upper bainite, carbides precipitate from austenite enriched in carbon, while in lower bainite, carbides also form within ferrite plates (Bhadeshia, 2019). The bainite transformation is generally accepted as diffusionless, with the possibility of carbon diffusion from bainitic ferrite to retained austenite or carbide precipitation. The process resembles nucleation and growth, with sheaves forming through the accumulation of sub-units initiating at grain boundaries.

The presence of alloying elements and the slow cooling rates typical of large industrial sections, such as ingots or the core of forgings, can promote other morphological variants,

where carbon diffusion plays a more dominant role. This includes globular or granular bainite. This variant is typically characterized by non-acicular, more rounded ferrite units. It is commonly seen in low-carbon or low-alloy steels under prolonged holding times or very slow cooling, as carbon partitioning is less restricted(Bhadeshia, 2019).

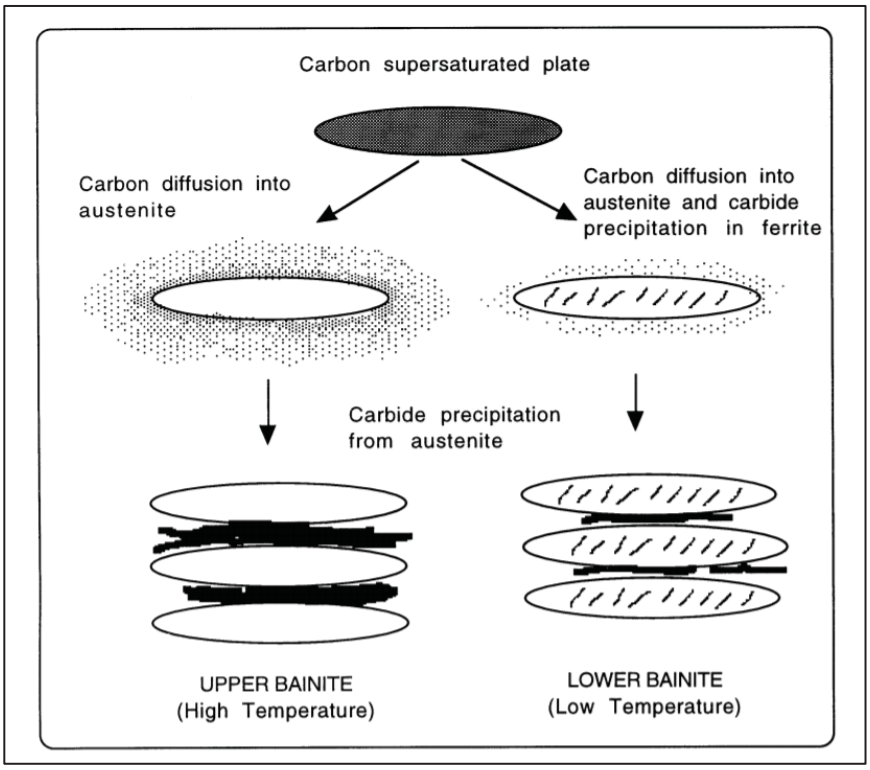

Figure 1.5 Schematic representation of difference between upper and lower bainite Taken from Bhadeshia (2019)

1.1.4 Austenite

Austenite is a high-temperature phase in steel and iron-carbon alloys, characterized by its face-centered cubic (FCC) crystal structure. It is named after Sir William Chandler Roberts-Austen, a British metallurgist who made significant contributions to the field of metallurgy. Austenite typically forms at temperatures above 912°C for pure iron and at varying temperatures for different steel compositions. For plain carbon and low alloy hypoeutectoid steels ($C \leq 0.77\%$), it forms above the A_3 critical temperature, which ranges from 727 °C to 912 °C depending on the carbon content. For hypereutectoid steels ($C > 0.77\%$), full austenitization occurs above

the A_{cm} line, which can extend to over 1147 °C. This phase can dissolve a considerable amount of carbon, up to 2.14% by weight at 1147 °C. The high solubility of carbon in austenite is a crucial factor in heat treatment processes for steels.

In most steels, austenite is not stable at room temperature and transforms into other phases such as ferrite, pearlite, or martensite upon cooling. However, in certain alloy compositions, especially those containing high levels of nickel and manganese, austenite can be retained at room temperature(Callister & Rethwisch, 2018). These steels are known as austenitic stainless steels and are valued for their excellent corrosion resistance and non-magnetic properties. Austenite formation is a critical process in the heat treatment of steel and iron-carbon alloys, significantly influencing the final properties of these materials. Understanding various factors, such as the initial phase, grain size, heating rate, and their interplay, is essential for optimizing heat treatment processes and developing advanced steel grades with enhanced mechanical properties. The ability to control austenite formation opens possibilities for creating steels with tailored microstructures suited for a wide range of applications, from automotive components to construction materials(Speer & Processing, 2018).

1.2 Factors affecting austenite formation

Austenite formation in steel and iron-carbon alloys is influenced by several key factors, operating under two primary types of heating: continuous heating and isothermal holding. The initial microstructure, whether it be ferrite, pearlite, bainite, or martensite, plays a significant role in the transformation process. The starting grain size also affects the formation of austenite, as does the heating rate applied during continuous heating. When considering continuous heating, a faster rate can suppress certain transformations or lead to finer austenite grains(Speer & Gaster, 2018).

Chemical composition is another crucial factor, as different alloying elements can impact the austenite formation kinetics, influencing both continuous heating transformations and the time required for isothermal holding. Additionally, the austenitizing temperature and holding time

are critical parameters that determine the extent and uniformity of austenite formation, mainly during isothermal holding. During isothermal holding, the material is rapidly heated to a specific temperature and then maintained at that temperature for a set duration, allowing the transformation to proceed to completion. These factors collectively influence austenite grain nucleation, growth, size, distribution, and homogeneity. Understanding and controlling these parameters, whether through continuous heating or isothermal holding, is essential for optimizing heat treatment processes and achieving desired material properties in steel and iron-carbon alloys(Roosz et al., 1982).

1.3 Heating Rate

The heating rate significantly influences the mechanism and kinetics of austenite formation, leading to diverse microstructural outcomes. This influence stems primarily from how heating rate affects the dominant diffusion mechanisms and, consequently, the growth rate of austenite. At higher heating rates, austenite formation kinetics are generally faster, often controlled by the rapid interstitial diffusion of carbon through the bulk material. This is in contrast to lower heating rates, where interface diffusion of substitutional alloying elements tends to govern the growth, leading to slower kinetics. For example, (Oliveira et al., 2007) observed that for the same initial microstructure, higher heating rates resulted in faster kinetics due to carbon volume diffusion, while lower heating rates showed slower kinetics governed by the interface diffusion of substitutional atoms as shown in Figure 1.6.

The critical temperature for austenite formation is also affected by the heating rate, a phenomenon often accompanied by a shift in the dominant growth mechanism. (Settimi et al., 2019) demonstrated this in alloy steel with a martensitic initial microstructure shown in Figure 1.7. They found that lower heating rates favored a diffusive growth mechanism, resulting in the formation of globular austenite with low dislocation density. On the contrary, higher heating rates promoted a displacive mechanism, leading to the formation of lath-shaped austenite grains with high dislocation density.

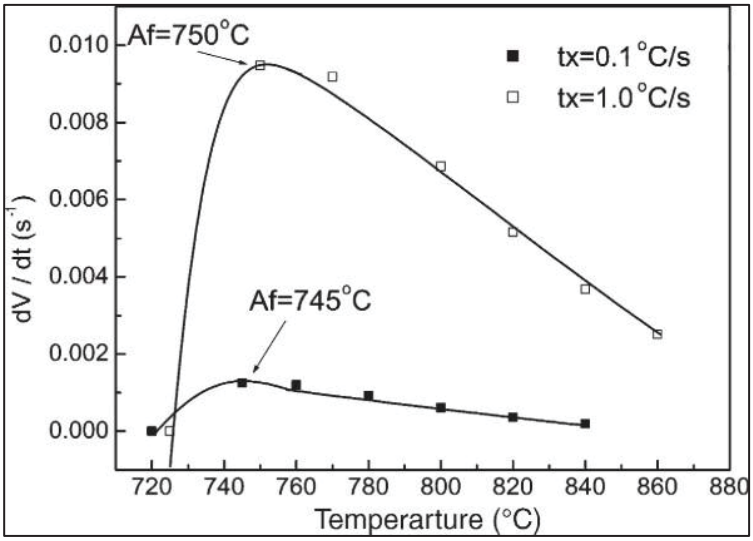

Figure 1.6 Rate of austenite volume formed as a function of temperature
Taken from Oliveira et al. (2007)

The heating rate can also dictate the number of stages involved in austenite formation. (López-Martínez et al., 2015) investigated micro-alloyed steel with bainite and martensite initial microstructures and categorized austenite formation as either a one-step or two-step process depending on the heating rate. High heating rates typically exhibited a single-step transformation, while lower heating rates resulted in a two-step mechanism.

(Yang, 1991)further explored the impact of heating rate on austenite formation from bainitic ferrite with retained austenite and tempered bainitic ferrite with carbides. At low heating rates, both microstructures showed similar kinetics because retained austenite had sufficient time to dissolve into ferrite and carbides, leading to a final microstructure resembling tempered martensite. However, at high heating rates, retained austenite remained stable until secondary austenite formation, and the pre-existing retained austenite in the starting microstructure grew without requiring nucleation, thereby accelerating kinetics for this microstructure.

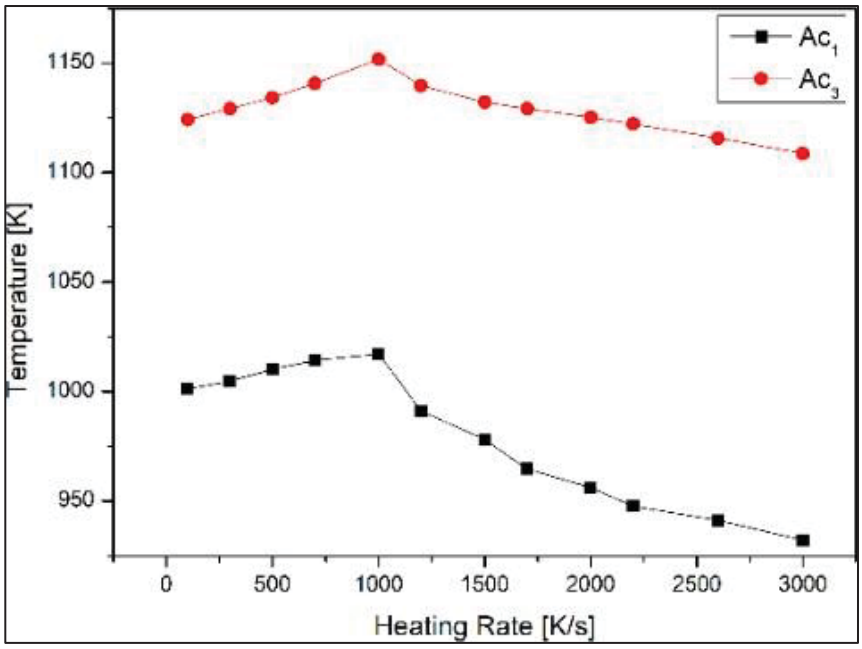

Figure 1.7 Change in critical temperature with heating rate
Taken from Settimi et al. (2019)

The JMAK (Johnson-Mehl-Avrami-Kolmogorov) equation coefficients are also influenced by the heating rate, reflecting the change in growth mechanisms. (Lopes & Cota, 2014) observed that for a pearlite + ferrite initial microstructure, austenite formation exhibited faster kinetics than a martensite starting phase at a slow heating rate of 0.1°C/s. However, this trend reversed at higher heating rates. Notably, the K coefficient in the JMAK equation increased with the heating rate, with a more significant increase observed for pearlite and ferrite, indicating a shift in the dominant growth mechanism with increasing heating rate.

1.4 Initial Microstructure

The initial microstructure significantly influences the kinetics and mechanisms of austenite formation. This literature review highlights how various microstructural parameters, including grain size and the phases present, impact austenite formation. Understanding these relationships is crucial for developing accurate mathematical models, given the distinct transformation behaviors observed in martensite and bainite compared to pearlite.

1.4.5 Impact of Initial Ferrite Grain Size

The initial ferrite grain size demonstrably affects the kinetics of isothermal austenite formation. (Mohsenzadeh & Mazinani, 2019) showed a clear correlation between initial ferrite grain size and austenite formation kinetics, with a noticeable effect in ferrite-cementite starting microstructures than in pearlitic microstructures Figure 1.8. Their study also observed that larger cementite particle sizes resulted in slower austenite formation kinetics. For continuous heating, (Ben Fredj et al., 2018) investigated medium-carbon low-alloy steel with bainitic ferrite and retained austenite, using two different prior austenite grain sizes. They found that a smaller initial grain size led to a higher nucleation rate of austenite due to the increased availability of nucleation sites. This underlines the importance of accurately describing the grain size in the initial bainitic microstructure for modeling purposes. Furthermore, (Yang & Huang, 1993) observed that the spatial distribution of ferrite plates in acicular ferrite and bainitic ferrite microstructures differed, leading to slower austenite transformation in acicular ferrite compared to bainitic ferrite at a given isothermal holding temperature.

1.4.6 Influence of Initial Phases

The types of phases present in the initial microstructure exert a substantial influence on austenite formation (Garcin et al., 2017) compared to bainitic and martensitic parent microstructures in low-carbon steel during continuous heating. While the critical temperatures for austenite formation were not significantly affected, the final austenite grain size at high temperatures was. The bainitic parent structure yielded a finer austenite grain size than the martensitic initial microstructure, attributed to the cementite particles in bainite acting as effective nucleation sites. The presence of nano-metric precipitates in bainitic structures was also found to accelerate austenite formation kinetics.

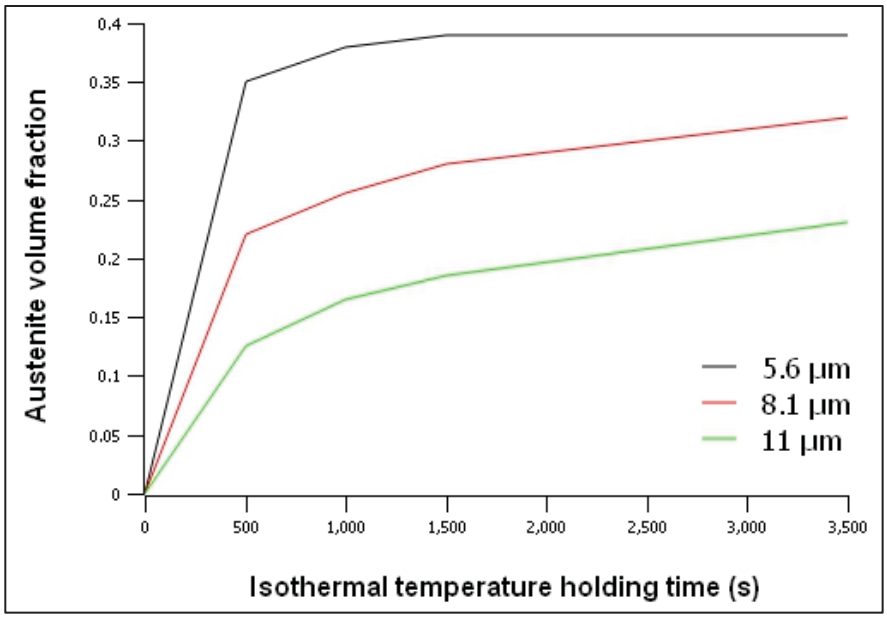

Figure 1.8 Volume fraction of austenite measured experimentally as a function of holding time at the inter-critical temperature of 740 °C for ferrite-cementite microstructures
Taken from Mohsenzadeh & Mazinani (2019)

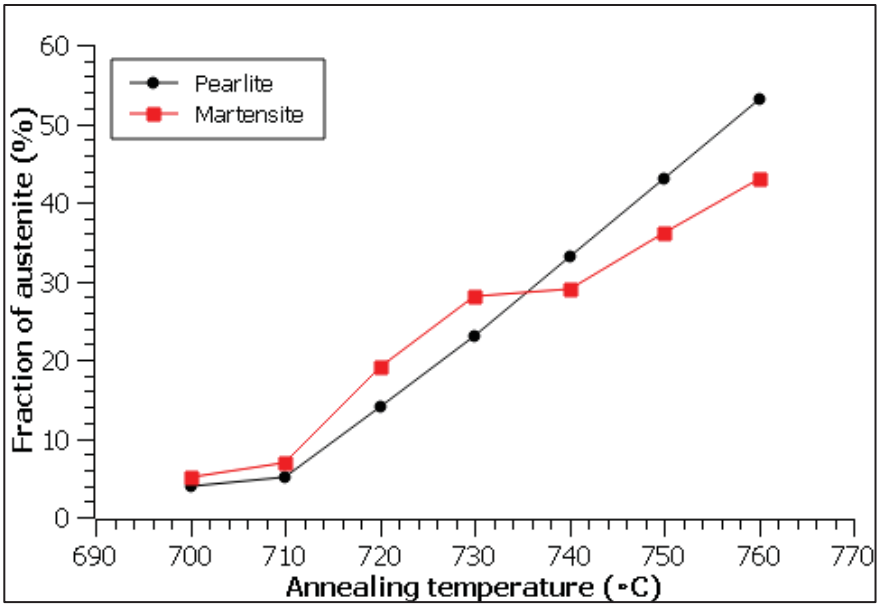

Figure 1.9 Changes in the austenite fraction of pearlite, and martensite as a function of annealing temperature
Taken from Dannoshita et al. (2019)

(Esin et al., 2014) investigated austenite formation kinetics across three different initial microstructures: ferrite-pearlite, bainite, and tempered martensite, under various heating rates.

They identified a two-stage austenite formation process for all microstructures: (i) simultaneous dissolution of ferrite and cementite, followed by (ii) exclusive ferrite dissolution. The extent of ferrite dissolution in the latter stage was significantly influenced by the heating rate for ferrite-pearlite and tempered martensite, but not for bainite. While heating rate affected austenite formation kinetics in ferrite-pearlite, its impact was less prominent for bainite and tempered martensite (Figure 1.9).

(Dannoshita et al., 2019) further explored the impact of initial microstructures (ferrite-pearlite (P), bainite (B), and martensite (M)) on austenite formation kinetics during inter-critical annealing. They observed that the initial phase significantly altered the kinetics Figure 1.9. A notable change in kinetics occurred after 740°C, attributed to a change in mechanism. Below 730°C, nucleation and growth of austenite proceeded under local equilibrium in pearlite specimen, while it occurred under para-equilibrium in martensite specimen. Above 740°C, austenite growth progressed under local equilibrium in all specimens. This highlights that both the initial phase and isothermal holding temperature dictate the mechanism, emphasizing the need to consider potential interactions between these parameters during modeling.

(Lopes & Cota, 2014) investigated austenite formation under isochronal conditions in Nb-microalloyed low carbon steel with ferrite-pearlite and tempered martensite initial microstructures at different heating rates. At a heating rate of 0.1°C/s, the ferrite-pearlite structure exhibited faster kinetics than martensite. However, at higher heating rates, martensite showed faster kinetics. This reversal in kinetics was attributed to a change in the mechanism of austenite formation: carbon diffusion controlled at lower heating rates, and interface-controlled transformation in ferrite-pearlite at higher heating rates. This again draws attention to the critical interplay between heating rate and initial microstructure, necessitating verification of parameter interactions for accurate modeling.

1.5 Mathematical Modelling

1.5.7 Mathematical Models of Austenite Formation During Isothermal Holding

The kinetics of austenite formation, a subject of extensive research over the past four decades, has been significantly advanced by the development of mathematical models. Early foundational work by (Speich et al., 1981) on inter-critical annealing of 1.5 wt.% Mn steel provided crucial insights into the multi-stage nature of austenite formation, which subsequently informed various modeling approaches. Speich's categorization of austenite formation into three distinct stages, rapid pearlite dissolution, slower ferrite transformation, and final homogenization of Mn through diffusion (as schematically illustrated in Figure 1.10) highlighted the critical role of temperature and the changing dominant diffusion mechanisms (carbon vs. substitutional elements).

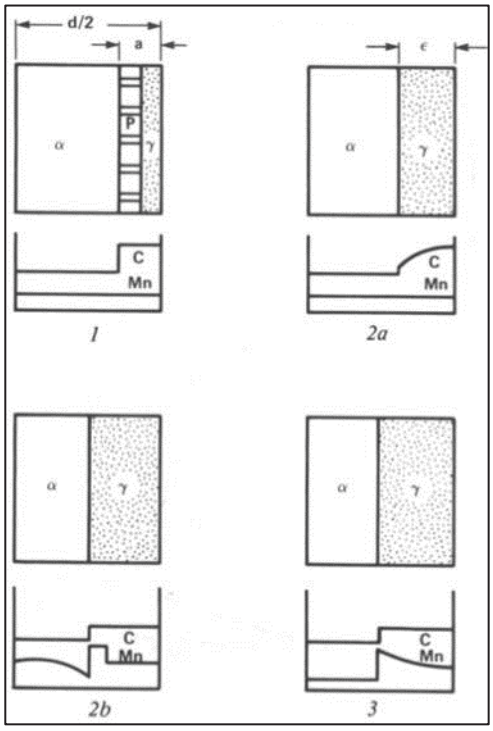

Figure 1.10 Schematic diagram showing three stages of austenite formation
Taken from Speich et al. (1981)

Mathematical models of austenite transformation are influenced by the underlying nucleation and growth mechanisms, which themselves are dependent on initial microstructure, temperature, heating rate, composition, and time.

Speich's initial modeling efforts for the first stage of austenite formation (growth into pearlite) employed a simplified one-dimensional slab models (Speich et al., 1981). This model assumed instantaneous nucleation of thin austenite films at the ferrite/pearlite interface, with subsequent inward growth of austenite. The time for pearlite dissolution, t_p, and volume fraction of pearlite V_p expressed as

$$t_p = {}^{a}/_{G} \; ; a = \; V_p \, {}^{d}/_{2} \tag{1.1}$$

with a being the half thickness of pearlite slab and d the diameter of the assumed cubic ferrite grain, and G is the growth rate derived from literature. Following pearlite dissolution, the model considered austenite growth into ferrite grains. In the absence of Mn diffusion, this growth was assumed to occur via carbon diffusion under paraequilibrium conditions, where equilibrium is considered only for carbon and not for Mn.

Building upon these mechanistic understandings, Roosz et al.(Roosz et al., 1982) developed one of the earliest comprehensive mathematical models for the kinetics of isothermal austenite formation in carbon steel with a fully pearlitic microstructure. Their model uniquely considered the characteristic features of the initial pearlite microstructure, assuming pearlite colonies as truncated octahedra (Figure 1.11). The kinetics of austenite formation, involving nucleation and growth, were described by the widely used Avrami equation:

$$X = 1 - \exp\left(-k_1 t^n\right) \tag{1.2}$$

where X is the transformed volume fraction, k_1 is a temperature-dependent constant, t is time, and n is a constant characterizing the kinetics. For an n -value of 4, obtained by fitting experimental data, both the nucleation rate ($\dot{N}$) and grain growth (G) are considered constant

with time (Christian, 2002). The constant k_1 was further related to these parameters by the equation

$$k_1 = \frac{\pi}{3}\dot{N}G^3 \tag{1.3}$$

Microstructural factors, specifically the structure factor

$$F = a_p\sigma_0 \tag{1.4}$$

(where a_p is the edge length of the truncated octahedron and σ_0 is the average inter-lamellar spacing of pearlite), were incorporated into the volume fraction calculation via the Avrami equation, leading to the plotting of a new type of austenitic isothermal diagram. Crucially, this model assumed sufficient nucleation sites and interface diffusion as the primary driver for growth, based on metallographic studies. The emphasis on interface diffusion explained compositional inhomogeneity of substitutional atoms due to its effect on carbon and substitutional element activity.

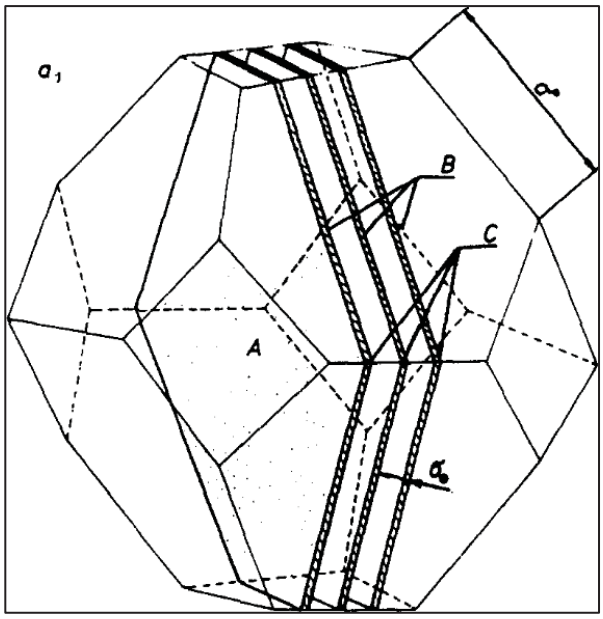

Figure 1.11 Pearlite colonies are seen as truncated octahedron
Taken from Roosz et al. (1981)

Further advancing analytical modeling, (Z. D. Li et al., 2011) presented a one-dimensional model for isothermal reverse transformation in pearlitic high-carbon hypoeutectoid steel. Their work revealed that the phase evolution during austenite formation is highly dependent on processing parameters, leading to three distinct types of evolution: cementite dissolution before ferrite, simultaneous dissolution of ferrite and cementite, or ferrite dissolution before cementite. This phenomenon, primarily observed in hypoeutectoid steel and not extensively addressed in prior research focusing on hypereutectoid steel, highlighted the critical role of isothermal transformation temperature. By exploiting the periodicity of the pearlite structure, their model focused on a single cementite lamella and a ferrite lamella, with austenite growing perpendicularly into both. The growth was defined by carbon diffusion, necessitating the application of Fick's law to calculate the rate of interface movement, thereby reflecting the kinetics of austenite formation. Mass balance equations served as boundary conditions (Akbay et al., 1994), and Thermocalc data was utilized for compositional calculations at specific temperatures. A limitation of this model, however, was its exclusive focus on growth rate, neglecting the nucleation rate.

More recently, (Z. Li et al., 2018) developed an analytical model for diffusion-controlled pearlite to austenite formation that concurrently considered the diffusion of solute elements through the volume of austenite and across the austenite-pearlite interfaces. Their model introduced the concept of a Pearlite-to-Austenite Transition Temperature (PNTT), above which austenite growth is predominantly governed by bulk carbon diffusion, and below which interface diffusion of substitutional atoms drives ferrite transformation into austenite. This illustrates the evolving sophistication of mathematical models, aiming to capture the complex interplay of diffusion mechanisms during isothermal austenite formation.

1.5.8 Mathematical Models of Austenite Formation During Continuous Heating

While much research has focused on the kinetics of austenite formation during isothermal transformation, the industrial relevance of continuous heating processes necessitates a thorough understanding and mathematical modeling of this phenomenon, for initial bainite and

martensite microstructures. Mathematical models for continuous heating generally fall into two categories: those derived from solving differential equations and those based on the Avrami equation, with some also incorporating dilatometric data fitting.

Early attempts to model phase change kinetics during continuous heating for multi-step diffusion processes, with varying growth rates and volume changes, include the work of (Dykhuizen et al., 1999). Their model calculated transient dilatation based on the fractional extent of different phases present, employing a self-calibration process to derive density variations from dilatometric data. While this model could predict austenite formation for any time-temperature path, a significant drawback was its lack of consideration for the influence of the initial microstructure, a factor now widely recognized as crucial.

The paramount influence of initial microstructure on transformation kinetics was subsequently addressed by (Caballero et al., 2001). Building upon the foundational model of Roosz et al. for defining initial microstructure, Caballero et al. extended it to continuous heating conditions. They leveraged theoretical knowledge from isothermal austenite transformation to develop a model applicable to non-isothermal austenite transformation in a wide range of steels, encompassing pure ferrite, pure pearlite, and mixed ferrite-pearlite initial microstructures. The Avrami equation was employed to describe austenite formation, with the nucleation rate (N) and grain growth (G) expressed as functions of activation energies, temperature, and functions representing the influence of initial microstructure and heating rate:

$$N = f_n(-\frac{Q_n}{k\Delta T}) \tag{1.5}$$

$$G = f_g(-\frac{Q_g}{k\Delta T}) \tag{1.6}$$

where Q_n and Q_g are the activation energies for nucleation and growth, respectively, k is the Boltzmann constant; and f_n and f_g are functions incorporating the influence of initial microstructure and heating rate. To account for overall austenite transformation under continuous heating, the Avrami equation was integrated over the entire transformation

temperature range, with time expressed as $t = \Delta T/\dot{T}$. This led to an equation for the volume fraction transformed at a given temperature (Vγ):

$$V_\gamma = 1 - \exp \int_{T_{A_{c1}}}^{T} \frac{4\pi}{3T^2} \dot{N} G^3 \Delta T^3 dT \tag{1.7}$$

$T_{A_{c1}}$ is the austenite start temperature. Their studies on eutectoid steel revealed that coarser pearlite leads to slower kinetics, and critical temperatures increase with heating rate, with a prominent effect on the austenite finish temperature. Equally, for finer pearlites, the influence of heating rate was less significant.

While initial studies often focused on hypereutectoid steels, (Gaude-Fugarolas & Bhadeshia, 2003) developed a model for hypoeutectoid steel, incorporating chemical composition, microstructure, and thermal history. They utilized classical nucleation theory to describe the nucleation rate, and diffusion-controlled growth to determine the progressive transformation of various phases into austenite. Austenite nucleation was considered to occur at the edges of pearlite colonies, growing until pearlite was completely consumed. The rate-limiting step was identified as the diffusion of carbon in austenite, emphasizing the significant role of morphology due to the large diffusion range. The model assumed that ferrite and cementite decompose together into austenite, thus their individual thicknesses were not considered. The nucleation rate in a single pearlite colony, based on classic nucleation theory, was given as (Christian, 2002):

$$I = CN \frac{6}{l} \frac{kT}{h} \exp\left(-\frac{G + Q}{RT}\right) \tag{1.8}$$

where N is the number of nucleation sites, C is a fitting parameter, k is the Boltzmann constant, T is temperature, G is the activation energy for nucleation, R is the gas constant, h is the Planck's constants. The growth rate was defined by carbon diffusion in austenite from the dissolving cementite to the austenite-ferrite boundary. Although initially designed for

isothermal transformations, this model was adapted for continuous heating by implementing it within a computer program that adjusted boundary conditions based on temperature changes. (Herrejón-Escutia et al., 2019) developed a semi-empirical model for austenite formation in pearlite and ferrite microstructures under continuous heating conditions. Their work showed that the dependence of the Johnson-Mehl-Avrami-Kolmogorov (JMAK) coefficient on heating rate varies. At lower heating rates, the n-value remained constant, allowing for the use of a diffusive JMAK model. However, at higher heating rates, the JMAK coefficient changed with heating rate, necessitating a non-isothermal rate model to describe the kinetics. For the growth of austenite into ferrite via diffusion, their model considered the homogenization of alloying elements.

(Vasilyev et al., 2019) presented a quantitative model for austenite formation under continuous heating, accounting for various compositions and microstructures. This model predicts the kinetics of austenite formation based on chemical composition, volume fraction of starting phases, ferrite grain size, and heating rate. Austenite nucleation sites were categorized into three modes, with corresponding variations in the nucleation rate equation. Importantly, this model assumed a negligible nucleation time for all modes. Growth rate was considered to be controlled by diffusion-controlled lattice reconstruction, though experimental validation for these assumptions was not explicitly provided.

It is evident that the majority of existing mathematical models for austenite formation during continuous heating primarily focus on pearlite and ferrite initial microstructures. Given the distinct variations in the transformation behavior of bainitic and martensitic microstructures compared to ferrite, there is a clear need for the development of mathematical models specifically tailored to describe austenite formation from these initial microstructures.

Current research on austenite formation kinetics from non-equilibrium microstructures, such as martensite and bainite, utilizes a multi-scale modeling approach to address the complexities of localized chemical and structural heterogeneities. Macroscopic studies commonly rely on modified Johnson-Mehl-Avrami-Kolmogorov frameworks and semi-empirical continuous

heating models to account for nucleation on preferential sites and growth (Pontevedra et al., 2019). Phenomena like carbon redistribution and the dissolution of inter-lath carbides are studied by multi-component diffusion simulations, such as those performed via DICTRA or Thermo-Calc (Enomoto & Hayashi, 2019). At the mesoscopic level, the Phase-Field Method and Cellular Automata are employed to simulate anisotropic grain boundary energies and preferential nucleation along lath boundaries (Erisir et al., 2015). Despite these advancements, a significant limitation persists in the current models that need to incorporate the initial microstructural influence, specifically prior austenite grain size. This study aims to address this research gap by quantifying the combined impact of initial grain size and accelerated heating rates on transformation kinetics.

1.6 State of the Art, challenges, and objective

Medium-carbon low-alloy steels are indispensable materials across a spectrum of critical industrial applications, ranging from vigorous landing gear components to high-performance hydraulic turbines. The exceptional mechanical properties and versatility of these steels are intrinsically linked to their microstructural evolution, especially the precise control of phase transformations during thermal processing. A cornerstone of this control lies in understanding the kinetics of austenite formation, a critical phase transformation that dictates the final microstructure and, consequently, the mechanical properties of the material. Existing metallurgical science has established the fundamental importance of optimizing thermal processing parameters to achieve desired microstructures and predict mechanical performance(Roosz et al., 1982). Techniques such as dilatometry and various microscopic characterization methods have been widely employed to study phase transformations. Mathematical models, often rooted in diffusion-controlled theories, have been developed to describe and predict these kinetic behaviors. However, despite significant advancements in the field, a comprehensive and nuanced understanding of austenite formation kinetics, especially when initiating from complex microstructures like bainite and martensite, remains an area requiring further in-depth investigation. The interplay between initial microstructure, such as

prior austenite grain size (PAGS), and dynamic thermal parameters like heating rate, has not been fully elucidated, representing a critical gap in the current state of knowledge. This gap is particularly pronounced regarding the specific influence of PAGS on austenite formation from an initial martensite microstructure, as well as the comparative kinetics and critical temperatures when starting from bainite versus martensite under varying heating rates.

The primary research challenge lies in achieving a better understanding of the kinetics of austenite formation from initial bainite and martensite microstructures in medium carbon low alloy steels. Specifically, the intricate interaction between prior austenite grain size (PAGS) and heating rate on these transformation kinetics presents a significant hurdle. While the individual effects of microstructure and heating rate on phase transformations have been studied(Settimi et al., 2019), their combined and synergistic influence on austenite formation from these specific non-equilibrium initial states is not well-documented or understood. A key challenge, as explored in this thesis, involves precisely characterizing the influence of prior austenite grain size on the kinetics of austenite formation in a medium-carbon, low-alloy steel with an initial martensite microstructure. Martensitic and bainitic microstructures are inherently complex, characterized by varying carbon distributions, dislocation densities, and crystallographic orientations, which affect nucleation sites and growth mechanisms during subsequent heating(Speer & Gaster, 2018). Quantifying these effects precisely and developing predictive models that accurately account for such complexities is challenging. A significant challenge involves establishing a clear distinction in the kinetics of austenite formation when the initial phase is bainite compared to martensite and understanding how the heating rate differentially impacts these transformations. The development of strong mathematical models capable of capturing the observed kinetic behaviors across a range of initial microstructures and heating rates, while also being refined by experimental data, will be a very useful tool for other researchers to further progress in this field.

To address the challenges and bridge the identified knowledge gaps, this thesis sets forth the following key objectives:

1. To quantify the influence of PAGS on austenite formation from initial martensite microstructure for medium carbon low alloy steels.

2. To investigate the influence of initial microstructure and heating rate on austenite formation from an initial martensite and bainite microstructure.

3. To develop a mathematical model to describe the kinetics of austenite formation starting from martensite and bainite microstructure.

To achieve these goals, samples will be prepared with 100% initial martensite or 100% initial bainite microstructure. The initial microstructure will be quantified by measuring the PAGS. The impact of the heating rate on critical temperature will be measured for bainite and martensite initial microstructures using high-resolution dilatometry. The predominant nucleation site will be identified for both bainite and martensite initial microstructures through intermittent quenching tests and microstructural characterization techniques (optical microscopy, SEM, and EBSD). The distinct novelty of this work lies in systematically isolating how variations in the initial PAGS impact austenite formation in martensite, a structural factor conventionally overlooked in existing literature, while clearly distinguishing the competitive transformation behaviors between martensitic and bainitic matrices under accelerated heating rates. The volume fraction of austenite formation will be mathematically modelled for continuous heating conditions for a given initial microstructure and heating rate. This model will be rooted in diffusion-controlled nucleation and growth theories and refined using a genetic algorithm to accurately describe and predict the extent of austenite formation. Through the fulfillment of these objectives, this research aims to provide novel, valuable insights for the precise control of thermomechanical processing in medium carbon low alloy steels, contributing to the optimization of their mechanical properties for industrial applications.

CHAPTER 2

MATERIAL AND EXPERIMENTAL METHODOLOGIES

2.1 Medium Carbon Low Alloy Steel

Steels are broadly categorized by their chemical composition into carbon steels and alloy steels. Carbon steels primarily rely on iron and carbon to dictate their properties, with further classification based on carbon content: low carbon (0.05 – 0.25 wt.% C), medium carbon (0.25 – 0.60 wt.% C), and high carbon (> 0.60 wt.% C). In contrast, alloy steels incorporate significant quantities of additional alloying elements, such as chromium, nickel, manganese, molybdenum, and vanadium, to enhance specific material properties. For instance, the superior corrosion resistance of stainless steel is attributed to its chromium content, which exceeds 10.5 wt.%. For the scope of this project, a medium carbon low alloy steel was selected. This class of steel is characterized by a carbon content typically ranging from 0.25 to 0.60 wt.%, along with the presence of several key alloying elements, such as molybdenum and chromium, each generally present at concentrations below 10 wt.%.

This specific material finds extensive application in critical engineering components, including landing gear and hydraulic turbines, owing to its balanced mechanical properties. Its relevance is highlighted by its use in the manufacturing processes of our industrial partner. The chemical composition of the steel investigated in this thesis is detailed in Table 2.1.

Table 2.1 General chemical composition of the steel used in this study (wt. %)

Fe	C	Mn	Si	Ni	Cr	Mo
Balance	0.26	1.00	0.35	0.60	1.45	0.55

2.2 Experimental Apparatus: High-Resolution Dilatometry

The kinetics of phase transformations in this project were primarily assessed using the DIL 805 A/D high-resolution dilatometer (Figure 2.1). This instrument is capable of detecting minute dimensional changes, with a resolution of 0.01 µm per 0.05 °C, across a broad temperature range spanning from 20 °C to 1700 °C.

Figure 2.1 Dilatometer DIL805 A/D
Taken from TA Instruments (2023)

For electrically conductive materials, heating is achieved through induction via a water-cooled copper coil, enabling rapid heating rates of up to 100 °C/s. To minimize high-temperature oxidation, a partial vacuum is maintained with the pressure of less than $4*10^{-4}$ mbar within the system both prior to and during heating, which ensured no oxidation during heating. Cooling is facilitated by the controlled release of inert gases, such as helium or argon, with a high purity level of 99.999%, directly onto the specimen through the copper coil. Both heating and cooling

cycles are precisely program controlled. Real-time temperature measurements are conducted using a K-type thermocouple, spot-welded to the surface of the specimen.

Dilatation measurements are performed using a differential pushrod system. The specimen is held between two rods: one fixed and the other connected to a linear variable differential transducer (LVDT). As the specimen undergoes thermal expansion or contraction, the LVDT detects these dimensional changes. The pushrods are constructed from fused silica for temperatures below 1200 °C and alumina for higher temperature applications. Unlike traditional radiation furnaces that heat both the specimen and the entire chamber assembly, the induction system used here focuses energy exclusively on the metal sample with a highly localized hot zone. Because the heat is confined to this small, specific area, the pushrod tips experience minimal thermal exposure. This approach effectively eliminates errors caused by pushrod expansion, ensuring the accuracy of the dilatometry measurements. The standard specimen geometry for these experiments is a cylindrical sample with a diameter of 4 mm and a length of 10 mm. The DIL 805 A/D system offers modular expandability, allowing for the integration of various specialized modules. These include a deformation module for mechanical testing, a sub-zero module for low-temperature transformations, a coefficient of thermal expansion (CTE) measurement module, and an optical dilatometry module for enhanced accuracy and the capability to measure radial dilatation.

2.2.1 Dilatometry Fundamentals

Dilatometry fundamentally involves measuring the change in length (dilatation) of a material during controlled continuous heating and cooling cycles. This technique is effective for studying phase transformations in materials like steel, where phases such as γ-iron (face-centered cubic, FCC) and α-iron (body-centered cubic, BCC) possess distinct specific volumes. The change in lattice structure during a phase transformation leads to a measurable change in the overall sample length as can be seen in Figure 2.2.

2.2.2 Determination of Critical Temperatures

By recording the specimen's dilatation as a function of temperature and time throughout a heat treatment cycle, critical transformation temperatures can be precisely determined. When plotting the change in length versus temperature, any significant change in slope that results in delineation of the curve from thermal expansion directly indicates an instability in the current phase, signifying the onset or completion of a phase transformation.

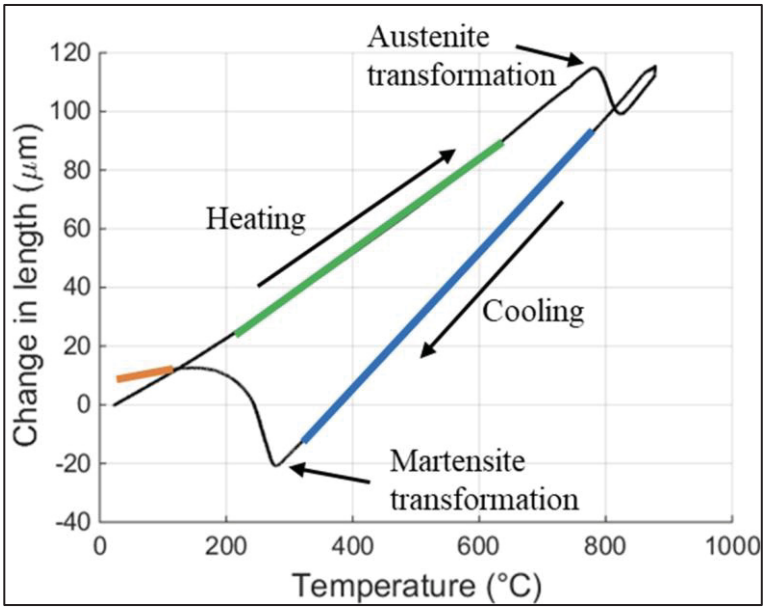

Figure 2.2 Typical dilatometry curve for a heat treatment cycle
Taken from Jia Hong LIU & Hong Liu (2023)

The coefficient of linear thermal expansion (CLTE), α_L, can be approximated from the slope of the dilatation curve with respect to the initial sample length, L_0, using the following expression (James, Spittle, Brown, & Evans, 2001):

$$\alpha_L = \frac{1}{L}\frac{dL}{dT} \tag{2.1}$$

where L is the given length, dL represents the instantaneous change in length, and dT is the instantaneous change in temperature. This approximation assumes a constant CLTE within the

given temperature range. Figure 2.2 illustrates a typical dilatometry curve for a quench process. The distinct slopes of the segments (e.g., green, blue, and orange lines) correspond to the CLTE of different phases, such as the base material phase, austenite, and martensite, respectively. The points at which these slopes change delineate the start and finish temperatures of the transformations.

2.2.2.1 Kinetics of Phase Transformation

The transition between distinct slopes on a dilatometry curve directly reflects the progress of an ongoing phase transformation. The extent of transformation, or the transformed phase fraction, can be quantitatively approximated using the lever rule. This method, commonly applied in dilatometric analysis (Mustak et al., 2016), calculates the fraction of a transformed phase.

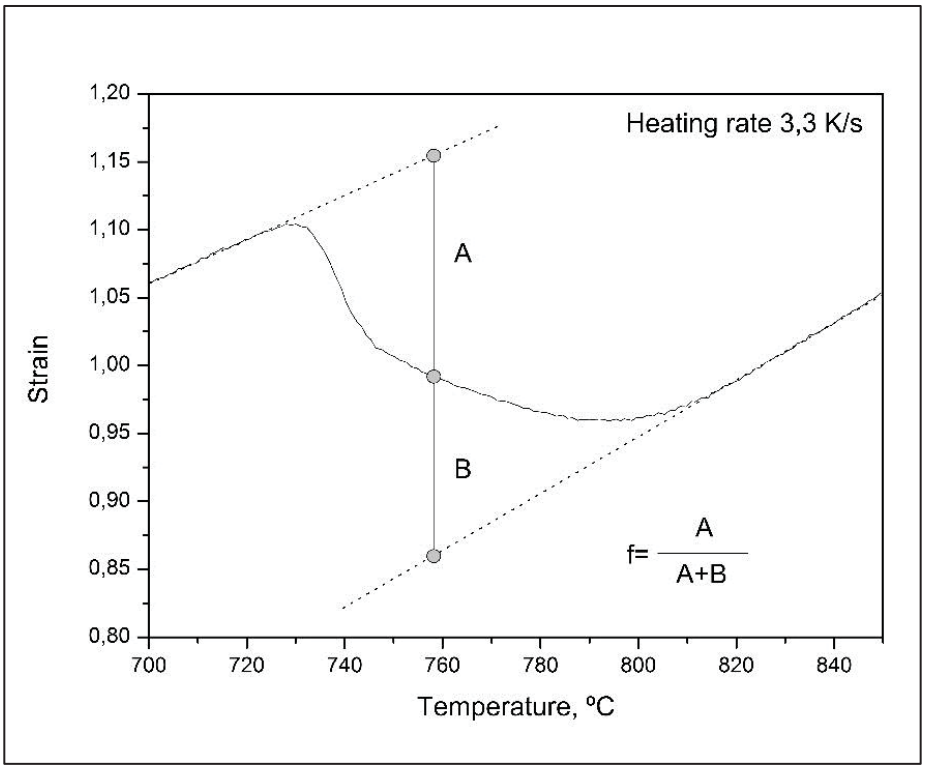

Figure 2.3 Determination of austenite volume fraction through dilatation curve using the Lever rule technique

Taken from Erisir et al. (2015)

As shown in Figure 2.3 for austenite transformation, the lever rule involves extending segments corresponding to the initial and final phase thermal expansion (represented by dashed lines). The fraction of the transformed phase at a specific temperature is then determined by the relative vertical distance between the measured dilatation curve and these extrapolated lines.

The simplicity of the lever rule makes it a convenient tool for analyzing dilatometric data. However, a key assumption of this method is that the final microstructure consists entirely of the transformed phase. Consequently, it may not accurately quantify residual phases, such as retained austenite (RA) at room temperature in martensitic transformations (Carlone et al., 2010) As such amounts cannot be directly determined from dilatometry curves alone.

2.2.3 Experimental Reproducibility

To ensure reproducibility, initial experiments were performed three times for the onset of austenite transformation to both small grain (SG) and large grain (LG) samples with initial martensite microstructure. The SG condition yielded Ac1 values of 757.3 ℃ on average with a standard deviation of 3.1 ℃, while the LG condition yielded values of 758.3 ℃ on average with a standard deviation of 2.1℃. Following this validation of machine stability, the remaining experiments were executed by single targeted runs, utilizing a spot-welded Type K thermocouple with an inherent standard limit of error of ±2.2 ℃ (ASTM E230).In addition, even when the uncertainty in the critical temperature is factored into the lever rule, the resulting error in the phase fraction remains low and is restricted almost entirely to the initial nucleation phase. During the steady-state growth period, this temperature variation has virtually no impact, because the extrapolated linear tangents are parallel, and any shifts in the baseline slope are mathematically offset. This confirms that the kinetic trends observed are true metallurgical developments rather than artifacts of experimental scatter.

2.3 Microstructural Characterization

To comprehensively understand the kinetics and mechanisms of phase transformations during continuous heating, dilatometry experiments were complemented by thorough microstructural characterization at various stages of the process. This included examining the initial microstructure, “freezing” intermediate transformation states by rapid quenching, and analyzing the final microstructure after complete heat treatment cycles. This multi-stage approach allowed for both direct evaluation and cross-validation of kinetic data obtained from dilatometry, as well as providing insights into the mechanisms of austenite formation under different initial microstructural conditions and heating rates.

2.3.4 Microscopy

Both optical and electron microscopy techniques were employed to observe and analyze the intricate microstructures of the steels under investigation. Selective etching procedures were

critical for chemically differentiating the various phases present within the microstructure. Once phases were identified, their spatial distribution and volumetric fractions could be quantified. Analyzing microstructures after controlled interruption of heat treatments provided invaluable insights into the dynamic processes of phase transformations and microstructural evolution.

For instance, Figure 2.4 illustrates how such analysis can reveal the amount and spatial distribution of formed austenite during inter-critical annealing. In such images, darker regions often correspond to martensite (representing the austenite phase at higher temperatures), while brighter regions indicate ferrite. This visual information allows for the quantification of transformed austenite at specific temperatures and times, directly supporting kinetic studies. The observation that martensite typically forms at grain boundaries in such images can reveal the primary nucleation sites for austenite formation. In this project, microstructures were captured immediately following the onset of austenite formation (as determined by dilatometry data) through rapid quenching. This approach is crucial for identifying early nucleation sites, which are vital for developing and validating phase transformation models. While optical and scanning electron microscopy were used to map the location and distribution of phases, these tools were used only to investigate localized nucleation and growth behavior. They were not used to determine total phase volume. Instead, all macroscopic phase fractions were calculated using high-resolution dilatometry to ensure the precision and accuracy of bulk volumetric measurements.

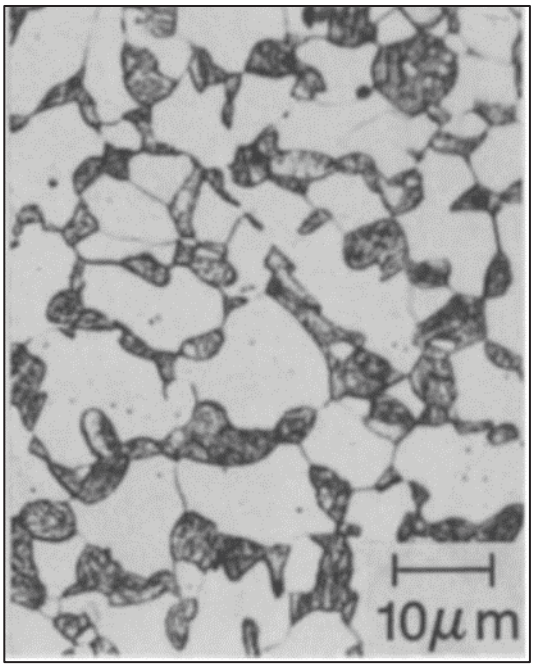

Figure 2.4 Microstructure after quenching from inter-critical annealing, bright area ferrite and darker area martensite (austenite)
Taken from Speich et al. (1981)

2.3.4.2 Electron Backscatter Diffraction (EBSD)

Electron Backscatter Diffraction (EBSD) is a powerful and versatile technique for detailed microstructural characterization and crystallographic analysis of crystalline materials. Beyond simply identifying phases, EBSD provides comprehensive data on the orientation and crystallographic texture of individual microstructural components. Several EBSD tools are relevant for understanding phase transformations in steels: phase mapping, Image Quality (IQ) mapping, and Kernel Average Misorientation (KAM) mapping. Phase distribution mapping generates real-time spatial maps of different crystal structures within the microstructure based on the electron diffraction patterns. This allows for clear differentiation between phases with distinct crystal structures, such as austenite (FCC) and ferrite (BCC). Image Quality (IQ) mapping reflects the quality of indexing of the diffraction patterns. Areas with higher internal strain or dislocation density, such as martensite, typically produce lower quality diffraction patterns, appearing as darker regions in an IQ map. This contrast can be exploited to differentiate phases. For example, within a ferrite-rich area, regions of martensite can be

identified as darker areas in an IQ map due to their high dislocation density and associated internal strains, while the surrounding unstrained ferrite appears brighter.

Kernel Average Misorientation (KAM) mapping quantifies the local misorientation within a defined kernel around each point relative to its immediate surroundings. This technique is effective for distinguishing between phases with similar crystal structures but different levels of internal strain or sub-grain boundary density. For instance, while both ferrite and bainitic ferrite are BCC, their transformation mechanisms and thermal histories result in bainite typically exhibiting a higher density of sub-boundaries or local misorientations compared to ferrite. KAM maps can highlight these differences. KAM maps with appropriate threshold values can effectively delineate ferrite from bainitic ferrite. Areas with a KAM value greater than a specific threshold are indicative of bainite, while areas below the threshold correspond to ferrite. The challenge lies in selecting the optimal threshold value, which is typically found when phase boundaries become smooth and scattered pixels disappear, indicating a reliable distinction. In summary, EBSD, through its combined capabilities of phase mapping, IQ mapping, and KAM mapping, serves as an exceptionally effective technique for analyzing phase transformations in steels. These methods enable precise quantification of the phases present in the microstructure, providing crucial data for evaluating transformation kinetics and understanding underlying mechanisms.

CHAPTER 3

KINETICS OF AUSTENITE FORMATION IN A MEDIUM-CARBON, LOW-ALLOY STEEL WITH AN INITIAL MARTENSITE MICROSTRUCTURE: INFLUENCE OF PRIOR AUSTENITE GRAIN SIZE

Navneeth Rajakrishnan [a,], Morteza Sadeghifar [a], Pinaki Bhattacharjee [b], Henri Champliaud [a], and Mohammad Jahazi [a]

[a] Department of Mechanical Engineering, École de Technologie Supérieure, 1100 Notre-Dame Street West, Montreal, QC H3C 1K3, Canada

[b]Department of Materials Science and Metallurgical Engineering, Indian Institute of Technology Hyderabad, Khandi, Sangareddy, 502284, India

Article published in Journal of Manufacturing and Materials Processing, January 2025, available at https://doi.org/10.3390/jmmp9010010

3.1 Introduction

High strength medium carbon low alloy steels are widely used in industrial products such as turbine shafts, landing gear, mold steel, etc. Most of these steels are manufactured through ingot casting, forging, and heat treatment. Heat treatment, often composed of a quenching and one or more tempering steps (Q&T), is a crucial stage that determines the final microstructures that decides the mechanical properties of the final parts. Among various factors, the phase transformations occurring during heating (i.e., austenite formation) and cooling (i.e., martensite, bainite or pearlite) play the most important role in determining the final mechanical properties of the material. While phase transformation during cooling has been extensively studied (Celada-Casero et al., 2019), it is only in recent years, with the advent of new generations of high strength steels, that much attention has been paid to the microstructural changes during heating, primarily austenite formation (Enomoto & Hayashi, 2018). Quantifying the impact of different microstructural constituents on the kinetics of austenite formation is of high interest from industrial as well as academic perspectives, to design more efficient and repeatable heat treatment processes, especially for high value-added components

such as aircraft landing gear. Specifically, for such applications, a fully martensitic structure is needed at the end of the quenching step. However, due to the thickness of the part, the austenite grain size, in the as-forged condition, is not uniform from the surface to the centre, and therefore, it is important to know how the kinetics of austenite formation is influenced by the initial grain size.

It is known that the austenite formation kinetics is affected by initial microstructural parameters such as the initial phase, grain size, and particle size. Dannoshita et al. (Dannoshita et al., 2019) studied the impact of three different initial microstructures with initial ferrite-pearlite (P), bainite (B), and martensite (M) phases in a low carbon steel. They found that during the inter-critical annealing, the kinetics of austenite formation varied with the initial phase. The isothermal holding at 740 °C demonstrated that the kinetics of austenite formation from initial ferrite-pearlite was quicker compared to that from the initial bainite microstructure, while the kinetics from initial martensite microstructure was the slowest among the three. The impact of the initial phase is apparent from the literature, which leads to the increase in studies on austenite formation from initial martensite microstructure.

The formation of secondary austenite from the initial martensite structure of a Fe-Ni-Mn alloy during heating was studied by Singh and Wayman (Singh & Wayman, 1987). They showed that the rate controlling mechanism were nucleation and growth through the long-range diffusional transformation. Enomoto et al. (Wei et al., 2013) studied the growth of austenite from as-quenched martensitic microstructure in a low carbon steel and identified lath and packet boundaries as the most favourable nucleation sites for austenite formation. Shinozaki et al. (Shinozaki et al., 2017) studied austenite formation of a Cr-Ni-Mo steel with slow heating rate with an initial tempered martensite microstructure. Two types of austenite nucleation were identified at lath boundaries, and at prior austenite grains and inside the grains. Nucleation at lath boundaries formed acicular austenite grains and nucleation at prior austenite grain boundaries or inside grains formed globular austenite grains. The austenitization for 18NiCrMo5 steel with initial martensite structure was studied by Settimi et al. (Settimi et al.,

2019). They reported a diffusive mechanism for low heating rates during austenite formation, whereas at high heating rates, the transformation was controlled by a displacive mechanism. Mohsenzadeh et al. (Mohsenzadeh & Mazinani, 2019) described that in a steel with the initial microstructure of ferrite and cementite particles, the increase in the average ferrite grain size caused a decrease in the kinetics of austenite formation. For a medium carbon low alloy steel, Fredj et al. (Ben Fredj et al., 2018) demonstrated that the nucleation rate increased with decreasing austenite grain size in an initial bainitic microstructure. Wang et al. (L. M. Wang et al., 2011) found that with the increase in the grain size in a nano-structured ferritic steel, both critical temperature and time taken for austenite formation increased. It is clear from the literature that the initial grain size plays a significant influence on the kinetics of austenite formation, but the studies considering the influence of the grain size did not address the phase transformation with initial martensite microstructure.

In recent years, there have been advancements in developing mathematical frameworks to analyse thermal processes associated with austenite formation, integrating thermodynamics with microstructural changes. The objective is to model treatment procedures accurately, employing kinetic models to predict the proportion of austenite. This approach aims to enhance precision in evaluating phase distribution within multiphase steel for designing microstructures.

The formation of austenite from ferrite-pearlite based initial microstructure has been modelled using Avrami, or Johnson–Mehl–Avrami–Kolmogorov (JMAK). Conventional models use thermodynamic equations to identify the kinetics parameters k and n (García De Andrés et al., 2001; Roosz et al., 1982). The kinetics of austenite transformation from pearlite for an isothermal transformation and a continuous heating condition was studied by Roosz et al. (Roosz et al., 1982) and Garcia et al. (García De Andrés et al., 2001), respectively. Both groups used the Avrami equation to quantify the kinetics of austenite formation and expressed k and n as a function of nucleation and growth rates. In contrast, the determination of kinetics parameters with iteration, linear regression, or multiple regressions is based on experimental data, which were generally obtained through dilatometry (López-Martínez et al., 2015;

Oliveira et al., 2007). Oliveira et al. (Oliveira et al., 2007) experimentally studied the kinetics of pearlite to austenite transformation in a low carbon steel using different heating rates. They observed that the k value depends on the heating rate, while the n value is independent of the heating rate. Lopez-Martinez et al. (López-Martínez et al., 2015) carried out a dilatometric analysis on the kinetics of austenite formation from bainite-martensite initial microstructure for heating rates less than 1 $℃/s$. They found that both kinetic parameters k and n increased with an increment in the heating rate. The authors explained the change in kinetics parameters with the change in growth mechanism during austenite formation. However, any of the above models did not directly consider the influence of prior austenite grain size of martensite before phase transformation.

The isothermal formation of austenite as a function of the grain size was modeled by Roosz et al. (Roosz et al., 1982). The authors studied pearlite to austenite transformation in a carbon steel. They reported that the nucleation rate was inversely proportional to the product of the average pearlite colony edge length with the square of the average true interlamellar spacing. Adopting the model developed by Roosz et al. (Roosz et al., 1982) to suit continuous heating experiments, Caballero et al. (Caballero et al., 2001) provided a mathematical model for the kinetics of non-isothermal ferrite-austenite transformation. They showed the Avrami equation can be used to model the kinetics of ferrite to austenite transformation.

The present research study aimed to investigate the kinetics of austenite formation of non-isothermal martensite-austenite transformation as a function of prior austenite grain size. Based on experimental results, a mathematical formulation was derived for this transformation kinetics by considering the nucleation sites and the growth of newly formed austenite grains. A combination of high-resolution dilatometry experiments, optical and electron microscopy as well as EBSD was used for this investigation. In addition, the mathematical modelling was conducted based on the fundamental mechanisms governing nucleation and growth on interfaces and the kinetics parameters were calibrated with genetic algorithm optimization. There was excellent agreement between the mathematical model developed by modifying a ferrite model and the experimental results.

3.2 Methodology

In this section, first, the material and the parameters employed for the preparation of the initial martensite sample with different prior austenite grain sizes, dilatometry studies, intermittent quenching, and microstructural characterisation are described. Then, the Genetic Algorithm method which was required to identify the kinetic parameters of the mathematical model defining the kinetics of austenite formation is explained.

3.2.1 Materials and methods

The material studied in this work is a medium carbon low alloy steel, with a nominal composition shown in Table 3.1. The material was provided by Finkl Steel-Sorel, Quebec, Canada. Cylindrical samples with 10 mm in length and 4 mm in diameter were prepared for dilatometry experiments. The Bahr 805D/A high-resolution dilatometer was used to carry out the heat treatment for the preparation of initial microstructure, continuous heating dilatometry experiments, and intermittent quenching experiments.

To replicate different locations in an industrial size forged block, specific thermal cycles were selected to establish an initial microstructure characterized by a martensitic matrix with two distinct prior austenite grain sizes. The selected heating rate was set at 5 °C/s and the cooling rate at 10 °C/s, with two different isothermal holding durations of 5 and 240 min, as illustrated in Figure 3.1. The specimen subjected to a shorter isothermal holding time of 5 min exhibited smaller grain sizes (SG), while the sample with an extended isothermal holding time of 240 min displayed larger grain sizes (LG). The SG samples represent the grain sizes of the outer surface of the industrial size forged block, and the LG samples represent those of the center.

The continuous heating experiments were conducted to analyze the kinetics of austenite formation at a heating rate of 5 °C/s for both the SG and LG samples. The austenite start and finish temperatures, as well as its volume fraction in the inter-critical region, were determined by dilatometric experiments (Ranjan & Singh, 2019).

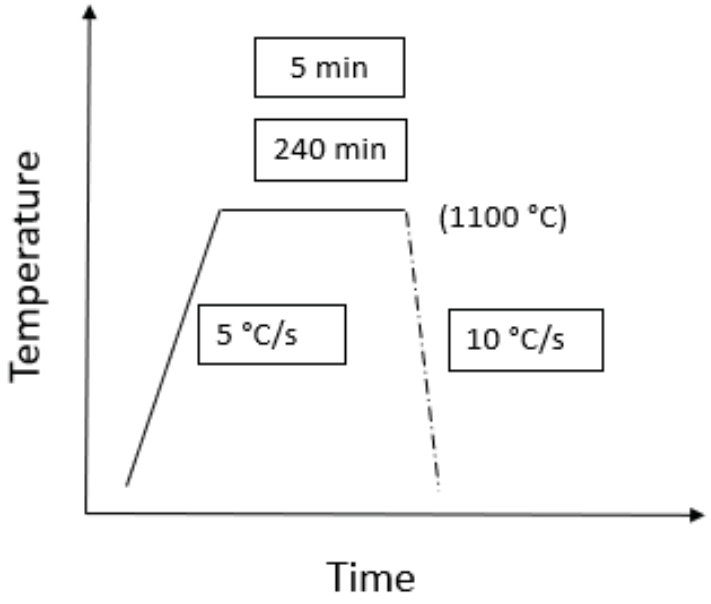

Figure 3.1 The thermal cycle with two different isothermal holding time for initial martensite formation.

Table 3.1 Chemical Composition of medium carbon low alloy steels in mass percentage.

C	Mn	Si	Ni	Cr	Mo	Fe
0.26	1.00	0.35	0.60	1.45	0.55	Balance

To investigate the microstructure during austenite formation and gain insights into nucleation and growth mechanisms, samples were quenched from the inter-critical region, allowing the high-temperature austenite to transform into martensite at room temperature. This quenching process, referred to hereafter as intermittent quenching, facilitated the examination of the austenite at room temperature. The intermittent quenching tests were carried out after heating the samples above Ac1 temperatures (780 and 790 °C) for the SG and LG samples, followed by immediate quenching using a helium gas. The heating rate employed was 5 °C/s, while the cooling rate was maintained at 40 °C/s.

The initial martensite microstructure and intermittent quenching microstructure were obtained by conventional chemical etching. Following the required heat treatment, the samples were prepared by grinding and polishing according to standard metallographic procedures. A chemical etchant, specifically 3 % Nital, was utilized in the process to reveal the features of the martensitic microstructure; however, it was not possible to reveal the prior austenite grains with Nital etching. To study the influence of initial martensite microstructure, it is essential to quantitively measure the microstructure by revealing the prior austenite grains. For steels with a low carbon content, chemical etching is not very effective at revealing prior austenite grains in heavily forged materials. Although the etchants such as Nital, Villela, and other etchants with picric acid as a base and a wetting agent, are commonly used for revealing prior austenite grains, they did not help reveal the prior austenite grains in this study (Garcıa de Andrés et al., 2002).

The thermal etching technique was therefore employed to reveal the prior austenite grains (Garcıa de Andrés et al., 2002). Initially, the as-received samples underwent standard metallographic procedures, including grinding and polishing. Subsequently, the as-polished samples were subjected to a heat treatment cycle that replicated the conditions of austenite formation in both the SG and LG samples. Upon exposure to high temperature, the prior austenite grain boundaries revealed by forming grooves that rendered them visible at room temperature under a light optical microscope.

The thermal etching technique involves exposing a pre-polished sample to high temperature in an inert atmosphere to expose the austenite grain boundaries. This process leads to the creation of grooves at the intersections of these boundaries with the polished surface. These grooves serve to adorn the austenite grain boundaries, allowing them to be observed at room temperature using a light optical microscope. This technique shows the austenite grains which were formed during the thermal simulation of the required heat cycle. The heat cycle used is the same as the one used for the preparation of the SG and LG samples. To find the PAGS of the SG sample, the sample was heated at 5 ℃/s up to 1100 ℃ and held at 1100 ℃ for 5 min before cooling down. For revealing the PAGS of the LG sample, the sample was heated at

5 ℃/s up to 1100 ℃ and held at 1100 ℃ for 240 min before cooling down. The thermal etching technique helped quantify prior austenite grains(Garcıa de Andrés et al., 2002). The prior austenite grain size of both the SG and LG samples was measured from the microstructure obtained by thermal etching, employing the standard method outlined in ASTM E-112.

The laser confocal microscope LEXT4100, a light optical microscope, was used in this study to analyze the microstructure after chemical etching and thermal etching. The microstructure after intermittent quenching was further analyzed by the SEM-EBSD technique using the SU8230 Hitachi Field-Emission Gun Scanning Electron Microscope equipped with Brucker FlatQuad detector. For the EBSD investigation, the samples were prepared using ion milling on a Hitachi IM4000-plus ion miller machine. Data acquisition was performed at an operating voltage of 25 KV, a working distance of 18 mm, and a step size of 0.16 µm. The post-processing of EBSD data was conducted using the ESPRIT 2.2 software.

3.2.2 Genetic Algorithms

Genetic Algorithm (GA) is a technique used for solving optimization problems. GA searches the design space based on random number generation using natural selection. GA is versatile and can be applied to various optimization challenges, predominantly those where the objective function is discontinuous, non-differentiable, stochastic, or highly nonlinear. It differs from classical, derivative-based optimization algorithms. The following outline summarizes how GA works (Sadeghifar et al., 2018).

i) The algorithm begins by generating a random initial population. Each population consists of an array of individuals, also known as chromosomes, genomes, or strings. Each individual is represented as a vector with entries referred to as genes, which are the design variables in the optimization process.

ii) The algorithm then generates a sequence of new populations. In each generation, the GA selects individuals with better fitness values from the current population, known as parents, to produce the next population, referred to as children. Three types of children are created:
Elite children: These are selected from the individuals in the current population with the highest fitness values. These elite individuals automatically survive to the next population. This process is known as reproduction.

Crossover children: These are created by combining the genes of a pair of parents. This operation, known as crossover, is typically applied with a high probability.
Mutation children: These are generated by applying random changes to a single parent. This operation, known as mutation, is applied with a low probability and helps prevent the GA from getting stuck in local minima.

The algorithm replaces the current population with the children to create the new population.

iii) The algorithm stops once the stopping criterion is met.

Moreover, some important terminology in GA is defined as follows:

“Population size” refers to the number of individuals present in each generation.

“Elite count” specifies the number of individuals guaranteed to survive to the next generation.

“Crossover fraction” specifies the fraction of the next generation, excluding elite individuals, that are generated by crossover. The remaining individuals in the next generation are produced by mutation.

“Function tolerance” refers to the threshold value. If the cumulative change in the fitness function value is less than this tolerance, the algorithm stops.

The mathematical model in this study that describes the kinetics of phase transformation for martensite to austenite transformation needed an optimization technique to identify the kinetic parameters based on the experimental results. GA described in this section was instrumental identifying the coefficients of kinetics parameters. In the following sections, details on how GA was applied to determine the coefficients of kinetics parameters were described.

3.3 Results and discussions

3.3.3 Initial microstructure

The SG and LG initial martensite microstructures were analyzed with the optical images shown in Figure 3.2. The microstructure obtained has a lath martensite microstructure with no apparent grain boundaries as seen after conventional etching. Figure 3.3 shows the microstructure with prior austenite grains revealed by thermal etching of the SG and LG samples. The SG sample has a prior austenite grain size (PAGS) of 117 μm, and the LG sample has a PAGS of 330 μm. The thermal etching technique simulated the required microstructure to obtain PAGS that could not be revealed by chemical etching.

3.3.4 Kinetics of austenite formation

Continuous heating experiments were carried out using the dilatometer to study the impact of PAGS on the kinetics of austenite formation. The thermal cycle used to prepare samples with two different grain sizes was designed in such a way that the SG samples had grain sizes close to that of the surface, and the LG sample had grain sizes close to that of the center of a 40 metric ton forged ingot. Therefore, the difference in kinetics between the SG and LG samples shows the difference in the kinetics of austenite formation in different parts of the forged ingot. The dilatometry curves of the SG and LG samples with a heating rate of 5 ℃/s are shown in Figure 3.4. The austenite start and finish temperatures were identified from the dilatometric curves. The beginning of contraction from the linear expansion marks the austenite start temperature and the end point of contraction that joins back to the linear expansion is the austenite finish temperature.

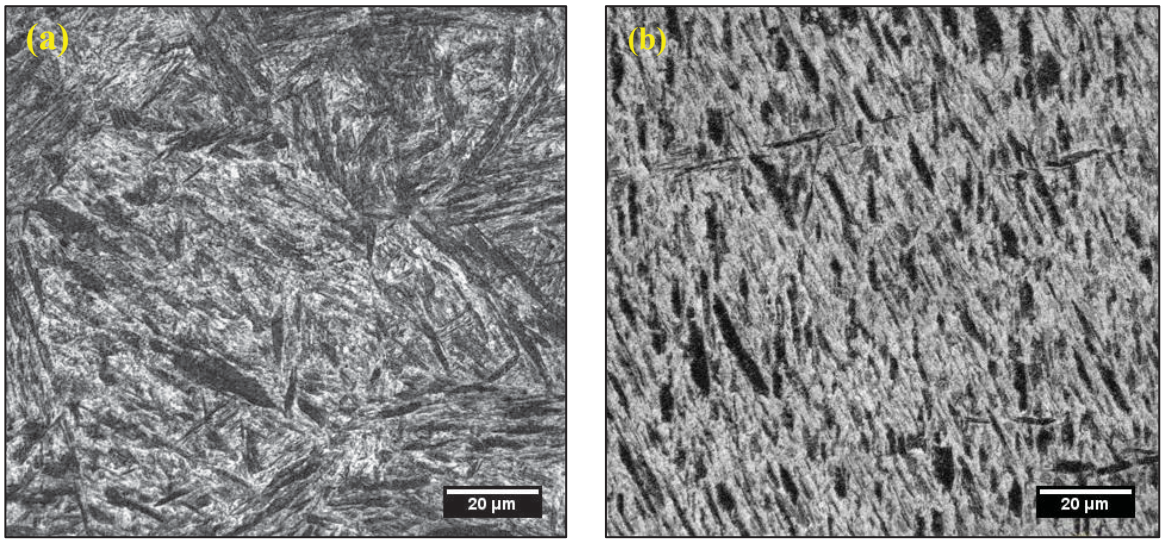

Figure 3.2. Initial martensite microstructure with: (a) 5-min isothermal holding and (b) 240-min isothermal holding.

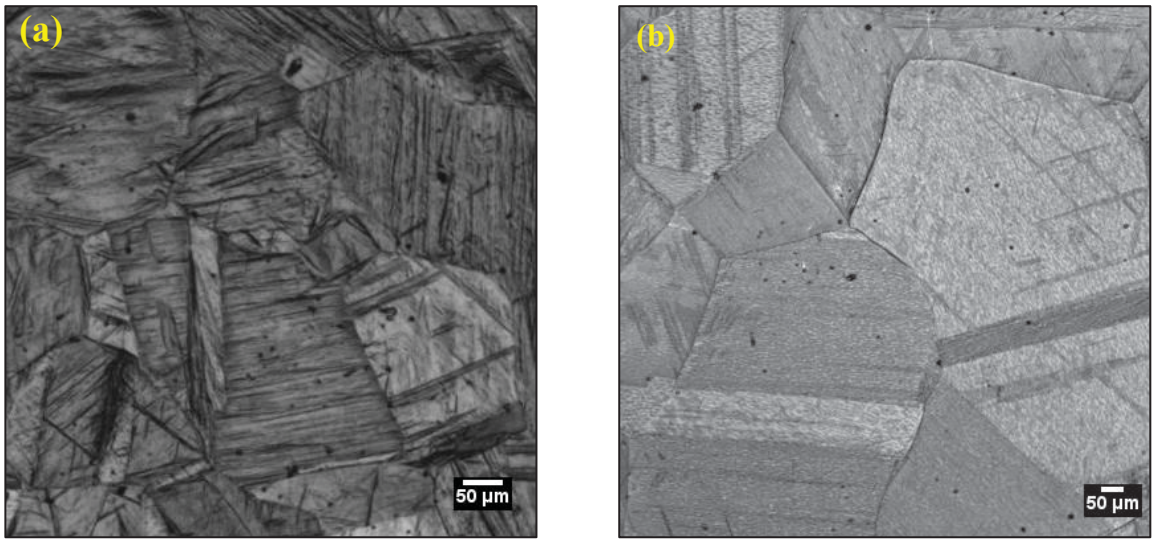

Figure 3.3 Thermal etching revealing prior austenite grain for: (a) 5-min isothermal holding at 1100 °C and (b) 240-min isothermal holding at 1100 °C.

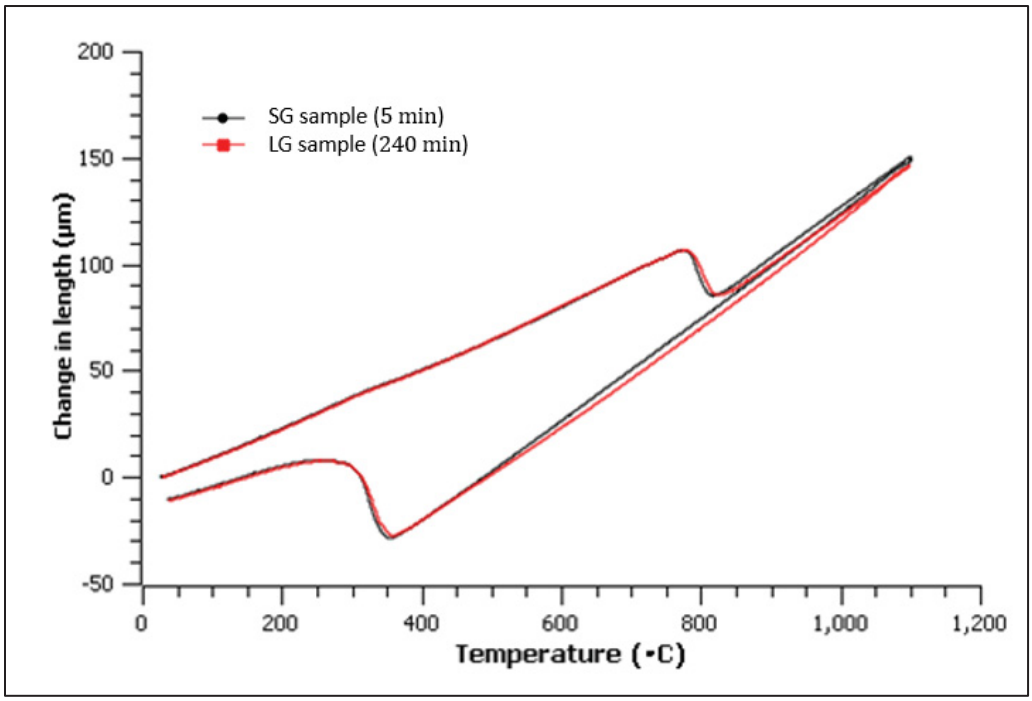

Figure 3.4 The dilatometry curves of the SG and LG samples.

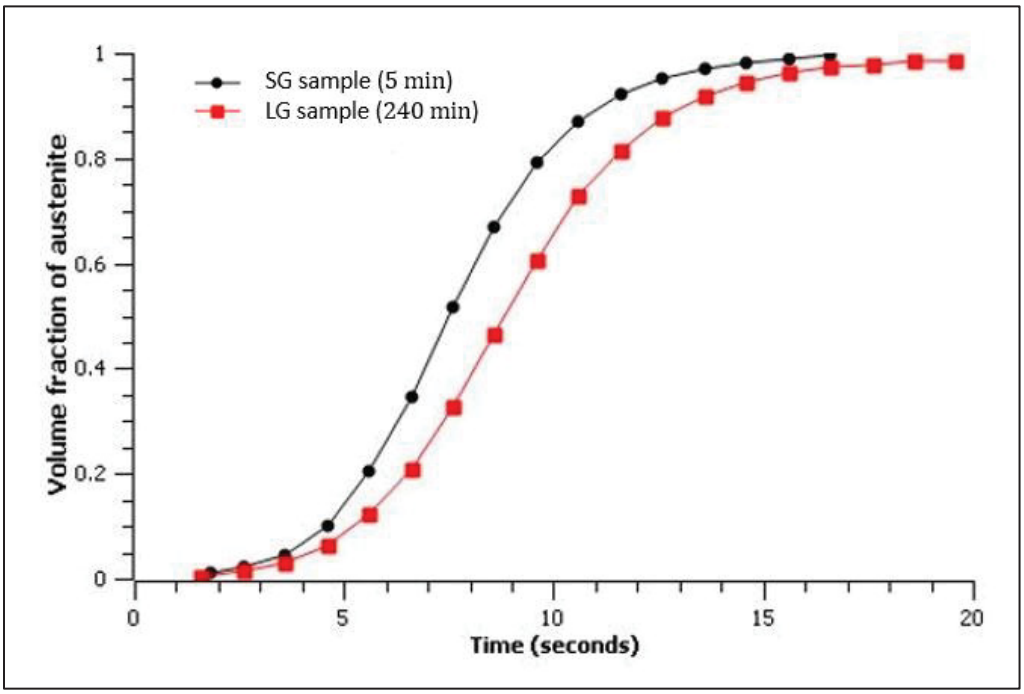

Figure 3.5 Kinetics of austenite formation for SG (5-min) and LG (240-min) samples.

Table 3.2 shows the values of the start and finish temperatures of both samples for a heating rate of 5 ℃/s. As seen in this table, there are no changes in austenite start temperatures with the change in PAGS of the initial martensite microstructure. These findings are in contrast with those of Wang et al. (L. M. Wang et al., 2011)who observed that the onset temperature of austenite formation (A_{c1}) was increased with increasing grain size in a nanostructured ferritic steel. The mechanically induced nanostructures have interfaces with high stored energy. The difference in stored energy because of changes in the grain size leads to an increase in critical temperature with an increase in the grain size. The SG and LG samples in annealed conditions, with an insignificant difference in stored energy, do not show the variation of critical temperature with a change in initial grain size.

Table 3.2 The critical temperature of the SG and LG samples heating at 5 °C/s

Transformation temperature (°C)	SG	LG
Start temperature	756	756
End temperature	820	816

Figure 3.5 shows the evolution of the volume fraction of austenite with time as a function of the grain size. The lever rule was applied to the dilatometry results at inter-critical temperatures to calculate the volume fraction of austenite. The results show that the SG samples, whose grains were finer, have faster kinetics than the LG samples with larger grains. The samples exhibit kinetic behavior depicted by an S-shaped sigmoidal curve. Initially, the transformation proceeds slowly until the formation of 10% austenite. Then, the growth accelerates rapidly until reaching 95% austenite. This rapid growth, evident in the linear middle segment of the sigmoidal curve, highlights the distinction between the SG and LG samples. As temperature rises, both the driving force for phase transformation and diffusion increase, leading to accelerated growth. The transformation rate (volume fraction of austenite formed with respect to time) eventually reaches a plateau, indicating the completion of the phase transformation.

3.3.5 Intermittent quenching

It is well known that the nucleation and growth mechanisms are responsible for austenite formation during heating.(Mattos Ferreira et al., 2023; Rezaei et al., 2023; W. Wang et al., 2022). The influence of nucleation and growth on the kinetics of austenite formation based on PAGS was analyzed with the help of the microstructures obtained from intermittent quenching. It is essential to know the nucleation sites for austenite formation to understand and quantify the kinetics of phase transformation. In the present work, intermittent quenching was performed at 780 ℃ and 790 ℃ for the SG samples and 780 ℃ for the LG samples in the inter-critical range to reveal the nucleation sites and growth of newly formed austenite grains.

Figure 3.6 shows the nucleation site of austenite on the SG and LG samples. The white region seen in the microstructure is high-temperature austenite that converted to martensite. (Roosz et al., 1982). Fig. 6(a) illustrates that austenite is nucleated on prior austenite grains for the SG sample. Fig. 6(b) displays that after quenching at 780 ℃, not only did most of the nucleation happen on the prior austenite grain boundaries in the LG samples, but there are also white spots that represent austenite nucleation inside the grains, in addition to those at grain boundaries. Fig. 6(c) demonstrates nucleation inside the grains for the SG samples at 790 ℃.

The above results indicate that at the beginning of the transformation, the preferential austenite nucleation site on martensite is at the prior austenite grain boundary. At higher temperatures, after site saturation on the prior austenite grain boundary, the secondary preferential nucleation site gets activated inside the grains. No experimental report is available on austenite nucleation sites in an initial martensite structure; however, the above findings agree with those of Speich et al.(Speich et al., 1981)who also reported that additional nucleation sites became activated as the phase transformation progressed in an initial pearlitic microstructure. In addition, they observed that nucleation occurred in pearlite colonies at temperatures just above Ac1, and as the temperature increased, nucleation sites were found at the ferrite – ferrite interface. (Speer & Gaster, 2018).

The EBSD analysis after intermittent quenching allowed us to identify the difference between the nucleation of the SG and the LG samples. The dark regions (non-indexed) on the band contrast images demonstrate the nucleation sites on grain boundaries. As the indexing of martensite (indicative of high- temperature austenite) is lower because of the inherent strain in the microstructure, the martensite appeared as non-indexed regions in Fig. 3.7. The Inverse Pole Figure (IPF) maps are depicted in Fig. 3.8. The SG sample has austenite growth seen as non-indexed regions, whereas the LG samples show growth seen as indexed regions. The IPF maps and band contrast images reveal that the strain energy associated with the nucleation of austenite is different between the SG and LG samples. It underlines the difference in nucleation pattern for the change in prior austenite grain size. Therefore, separate equations were formulated for each grain size.

3.3.6 Mathematical modelling

A mathematical model of the martensite to austenite transformation with the influence of an initial microstructure is presented in this section. As mentioned above, Caballero et al. (Caballero et al., 2001) proposed a mathematical model describing the non-isothermal ferrite-austenite transformation. They assumed nucleation at α/α grain boundaries and the nucleation sites on grain boundary faces, edges, and corners, all of which were considered as potential nucleation sites in their model. They also assumed that site saturation occurred during nucleation and the transformation was controlled by growth.

In the present work, the above model was modified to incorporate all the potential nucleation sites on the grain boundary. It must be noted that, based on the results reported in Fig. 6, it was also assumed that new austenite grains mainly formed at prior austenite grain boundaries. Cahn (Cahn, 1941.) reported that when nucleation occurs at the grain boundary at high nucleation rates, which is the case during the transformation of martensite to austenite, site saturation occurs, and the kinetics are controlled by the growth rate.

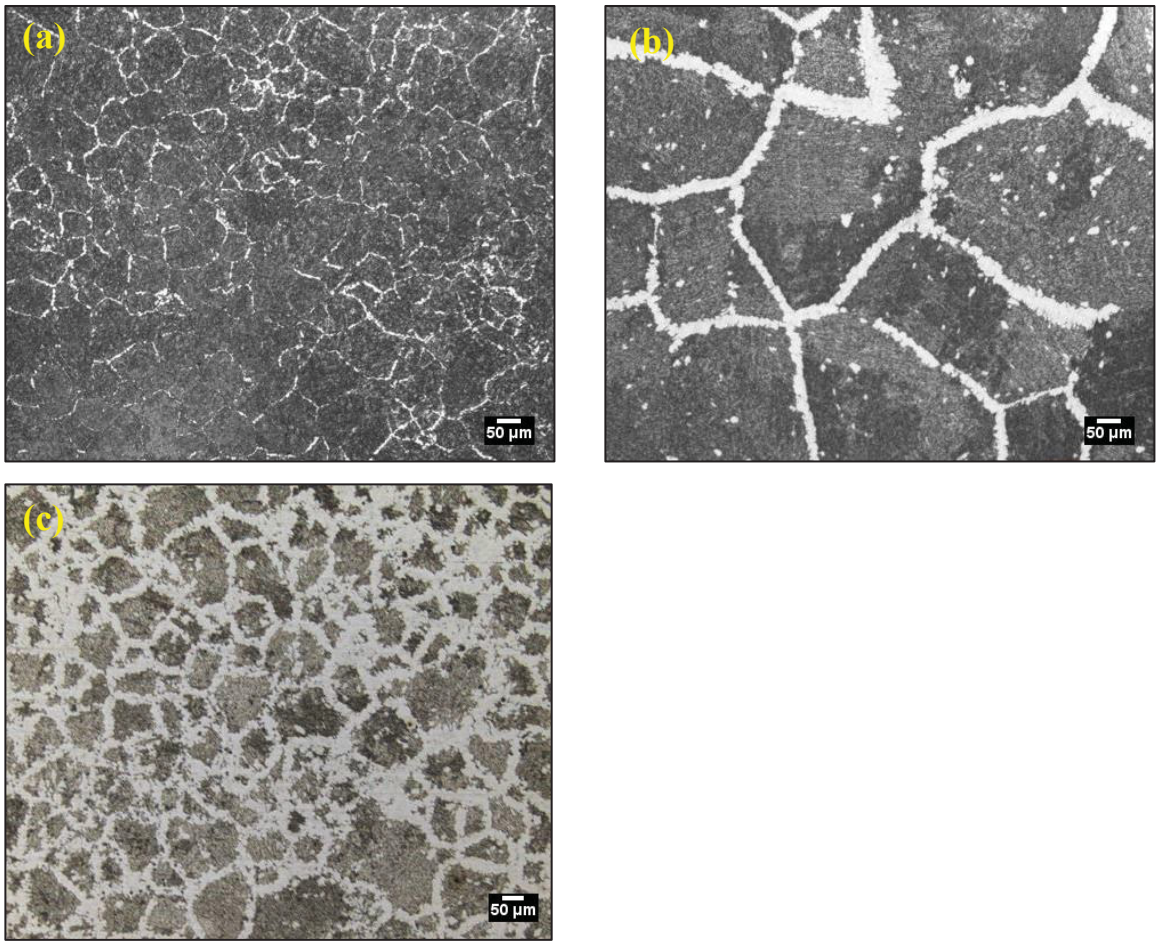

Figure 3.6 (a) The SG sample quenched at 780 °C, (b) the LG sample quenched at 780 °C, and (c) the SG sample quenched at 790 °C.

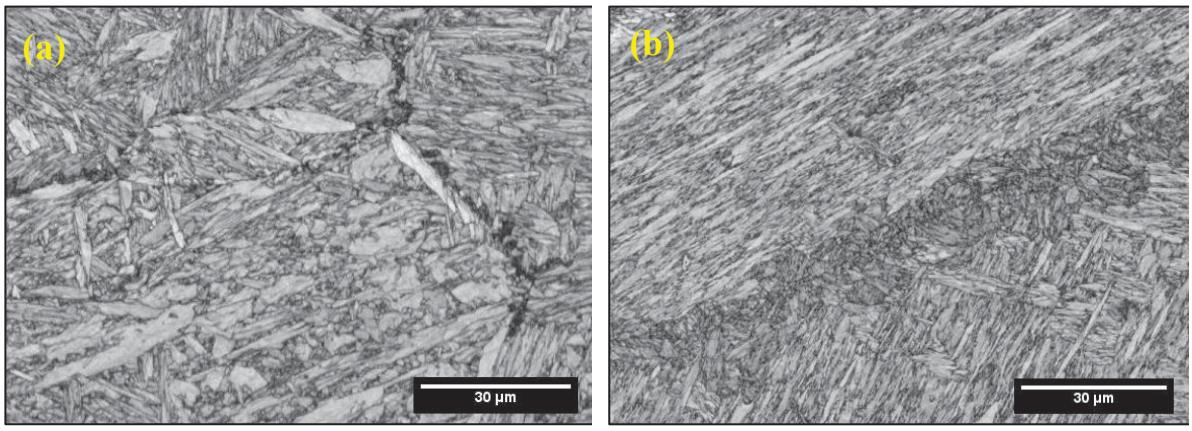

Figure 3.7 Band contrast image for (a) the SG sample and (b) the LG sample, showing austenite formation at grain boundaries.

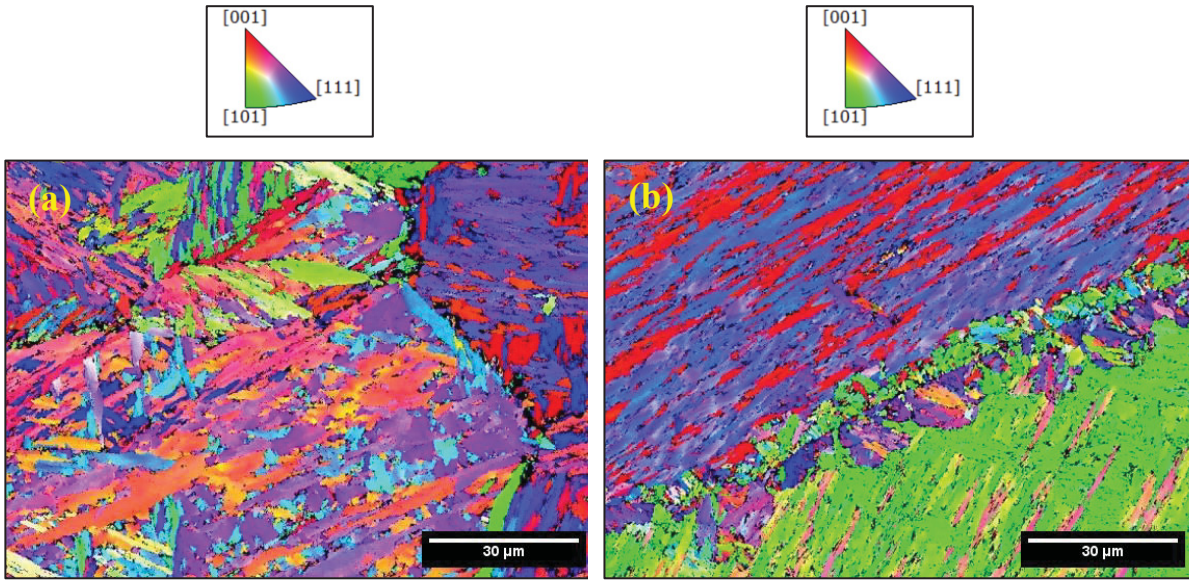

Figure 3.8 IPF maps for (a) the SG sample and (b) the LG sample, showing austenite formation at grain boundaries.

The growth rate can be calculated by the absolute reaction rate theory. (Christian, 2002). The growth is an interface-controlled process, and the growth rate G is given by:

$$G = \frac{\delta\vartheta}{kT}\exp\left(\frac{-\Delta G_{act}}{kT}\right)\Delta g^{\alpha\to\gamma} \tag{3.1}$$

$$G = \frac{\delta\vartheta}{kT}\exp\left(-\frac{\Delta S}{k}\right)\exp\left(-\frac{\Delta H}{kT}\right)\Delta g^{\alpha\to\gamma} \tag{3.2}$$

where δ is the boundary thickness equal to 0.5 nm [15], ϑ is the number of attempts to jump the boundary activation barrier per unit time, k is the Boltzmann constant, T is the absolute temperature, ΔG_{act} is the Gibbs energy for the activated transfer of atoms across the martensite/austenite interface, ΔS is the entropy of activation per atom, ΔH is the enthalpy of activation per atom, and $\Delta g^{\alpha\to\gamma}$ is the Gibbs energy difference per atom between the martensite and austenite phases. The value of ΔH is widely assumed to be equal to the enthalpy of activation for grain boundary diffusion (Paul Shewmon, 2016) and has been reported to be between -232×10^{-21} and -277×10^{-21} J/atom (Paul Shewmon, 2016).

In the present work, a ΔH value of -240×10^{-21} J/atom was determined to be suitable for both SG and LG samples. The assumed ΔH value is comparable to that of the ΔH values used in the literature (Paul Shewmon, 2016). The frequency of atomic jump ϑ is equal to kT/h, where h is Planck's constant. As reported in Table 3.2, the temperature at which austenite formation occurs is 1027 K. At this temperature, the value of ϑ was calculated to be $1.9 \times 10^{13}\ s^{-1}$.

The thermodynamic software package Thermo-Calc was utilized to compute the ΔS and $\Delta g^{\alpha \to \gamma}$. The graphical mode of Thermo-Calc was employed for this purpose. The database TCFe9 (steels: Fe alloys version 9.30) was used. The composition, as mentioned in Table 3.1, was specified in the system definer as input data. The difference in the entropy value between the austenite formation temperature and room temperature gives the entropy of activation. The ΔS calculated is 7×10^{-23} J/atom.

The Gibbs energy change for the BCC-FCC transformation $\Delta g^{\alpha \to \gamma}$ was calculated using the Thermo-Calc software. Figure 3.9 shows the variation of $\Delta g^{\alpha \to \gamma}$ as a function of temperature. It can be seen that with an increase in temperature, the difference in Gibbs energy between the BCC and FCC phases diminishes, indicating a rise in the stability of austenite and a reduction in the stability of the BCC phase. The $\Delta g^{\alpha \to \gamma}$ as a function of temperature was also calculated for ARMCO steel using the same technique, and the values were compared with those in the literature (Caballero et al., 2001). The values of $\Delta g^{\alpha \to \gamma}$ as a function of temperature from Thermo-calc are in good agreement with those in the literature, showing the reliability of the calculation technique used in this research.

The Gibbs energy value is expressed as a quadratic equation by fitting the obtained curve shown in Figure 3.9 as:

$$\Delta g^{\alpha \to \gamma} = (-3.7 \times 10^{-20} + 8.38 \times 10^{-21} T + 9.6 \times 10^{-22} T^2) \quad (3.3)$$

By inserting Eq. (3.3) into Eq. (3.2), the growth rate is calculated as:

$$G = \frac{85}{kT}(-3.7 \times 10^{-20} + 8.38 \times 10^{-21}T + 9.6 \times 10^{-22}T^2)\exp\left(-\frac{-240 \times 10^{-21}}{kT}\right) \quad (3.4)$$

The Avrami equation for growth kinetics with site saturation and three activated growth sites at grain boundary edges, grain boundary faces, and grain boundary corners can be expressed as [25]:

$$V_\gamma = 1 - \exp\left[-(k_s t + k_e t^2 + k_c t^3\right] \quad (3.5)$$

where V_γ represents the austenite volume fraction formed, t is the time, and k_s, k_e, and k_c are given by:

$$k_s = 2G\frac{S}{V}, k_e = \pi G^2 \frac{L}{V}, K_c = \frac{4}{3}\pi G^3 \frac{C}{V} \quad (3.6)$$

in which $\frac{S}{V}, \frac{L}{V}, and\ \frac{C}{V}$, respectively, are the boundary area, the edge length, and the grain corner number, all of which are per unit volume.

The model also must incorporate the prior austenite grain size. The ferrite model by Caballero et al. (Caballero et al., 2001) assumes that grains have a tetrakaidecahedra shape (i.e., a polyhedron with 14 faces). The same consideration is made in the present work based on the assumption that the nucleation sites are at grain boundaries from an equiaxed microstructure. The grains shaped like tetrakaidecahedra can effectively define nucleation sites at grain boundaries based on the grain size. Therefore, the assumption holds true. All grains are equally sized tetrakaidecahedra, and they fill space such that square faces are (100) planes and hexagonal faces correspond to (111) planes.

$$\left.\begin{aligned}\frac{S}{V}&=\frac{3.35}{D}\\ \frac{L}{V}&=\frac{8.5}{D^2}\\ \frac{C}{V}&=\frac{12}{D^3}\end{aligned}\right\} \tag{3.7}$$

And hence,

$$\left.\begin{aligned}k_s&=\frac{6.7G}{D}\\ k_e&=\frac{26.7G^2}{D^2}\\ k_c&=\frac{50.3G^3}{D^3}\end{aligned}\right\} \tag{3.8}$$

in which G is given in Eq. (3.4).

To address this equation for the non-isothermal reaction, the growth rate is expressed in terms of the assembly's state rather than the thermal path. Therefore, the time t is expressed as a function of temperature and heating rate, and the volume fraction is integrated over the given temperature, eventually yielding the equation for the volume fraction of austenite formed as:

$$V_\gamma = 1-\exp\{-\int_{T_s}^{T}[\frac{6.7}{\dot{T}D}G+\frac{53.4}{\left(\dot{T}D\right)^2}G^2(T-T_s)+\frac{150.8}{(\dot{T}D)^3}G^3(T-T_s)^2]dT\} \tag{3.9}$$

$$V_\gamma = 1-\exp\{-\int_{T_s}^{T}[\frac{A}{\dot{T}D}G+\frac{B}{\left(\dot{T}D\right)^2}G^2(T-T_s)+\frac{C}{(\dot{T}D)^3}G^3(T-T_s)^2]dT\} \tag{3.10}$$

The coefficients of the three activated growth sites are expected to be different for the SG and LG samples as their nucleation patterns are different. As a result, the coefficients of the three activated growth sites were replaced with variables A, B, and C, as shown in Eq. (3.10). As

seen in literature, the functional dependence of nucleation rate on grain boundaries, edges, and corners are constant while the coefficients were taken as approximate values(Cahn, 1956). In this study, the coefficients were optimized using the least squares optimization technique implemented with genetic algorithms, as detailed below.

3.3.7 Optimal design of the mathematical model

To obtain a mathematical model best fitted to the experimental data of the volume fraction of austenite for the SG and LG samples, it is required to find the optimal values of A, B, and C. The objective function was coded, and the optimization process was performed using the genetic algorithm (GA) solver provided in MATLAB®. The optimization problem was formulated as:

$$\begin{gathered}\text{Find } A, B, \text{ and } C \text{ to} \\ \text{Minimize } \sum\left(V_{\gamma,Exp} - V_{\gamma}\right)^2\end{gathered} \tag{3.11}$$

where A, B, and C are the design variables (see Table 3 for the GA results), and $V_{\gamma,Exp}$ and V_{γ} are the volume fraction of austenite at different temperatures from A_{c1} to A_{c3} measured in the experiments and modeled in the mathematical modeling (Eq. 3.10), respectively. In addition, $\sum\left(V_{\gamma,Exp} - V_{\gamma}\right)^2$ is the objective function defined based on the least squares technique (LST). It is required to explore a range of values for the GA elements to capture the most accurate optimum value. As a result, based on the user experience and the instructions in the GA user manual in MATLAB®, various values of "Population Size" ranging from 50 to 400, "Crossover Fraction" from 0.70 to 0.90, and "Elite Count" from 2 to 20were explored in the GA optimization tool. The number of "Generations", "Stall Generations", and "Function Tolerance" were set as stopping criteria in the GA tool to 500, 50, and 1×106, respectively. The optimum values of A, B, and C for each grain size are reported in Table 3. The calculated volume fraction using the mathematical model is plotted and compared with the experimental values, as shown in Figure 3.10.

Table 3.3 Coefficients of three activated growth sites calculated using the GA

Grain size (μm)	Coefficients of activated growth site		
	A	B	C
330	1	74.1	73.4
117	0.48	13.3	4

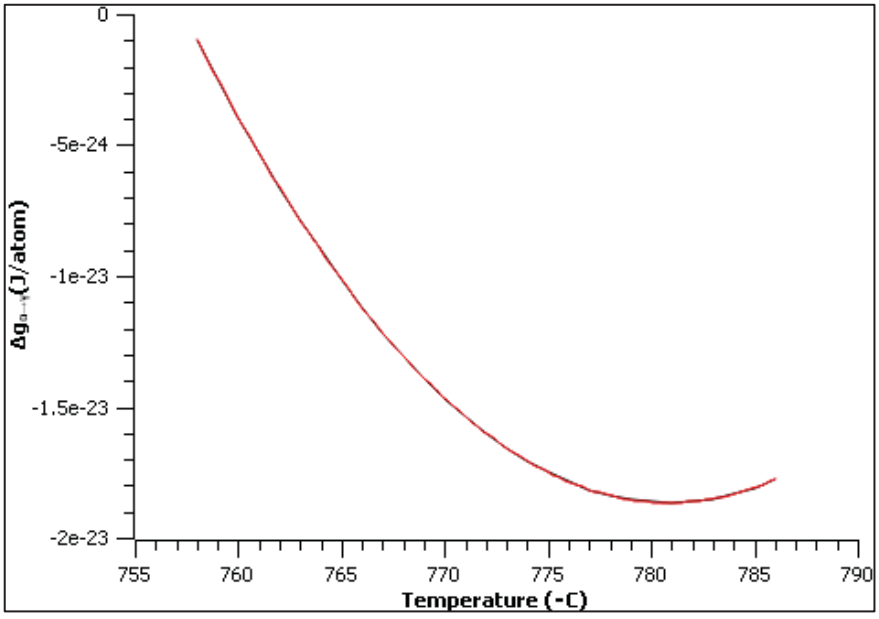

Figure 3.9. Gibbs energy difference per atom between the BCC and FCC phases calculated using Thermo-calc.

The predictive mathematical model is 0.99, demonstrating very good agreement between the mathematical model and the experimental results. The experiment and model for the LG sample differ in the first two seconds of the transformation. The model considers that rapid nucleation and growth rates control the kinetics of austenite formation. The LG sample exhibits a lower nucleation rate compared to the SG sample due to a smaller prior austenite grain boundary area, which acts as a nucleation site. This lower nucleation rate could explain the discrepancy between the modelling and experimental values for the first two seconds in the LG sample.

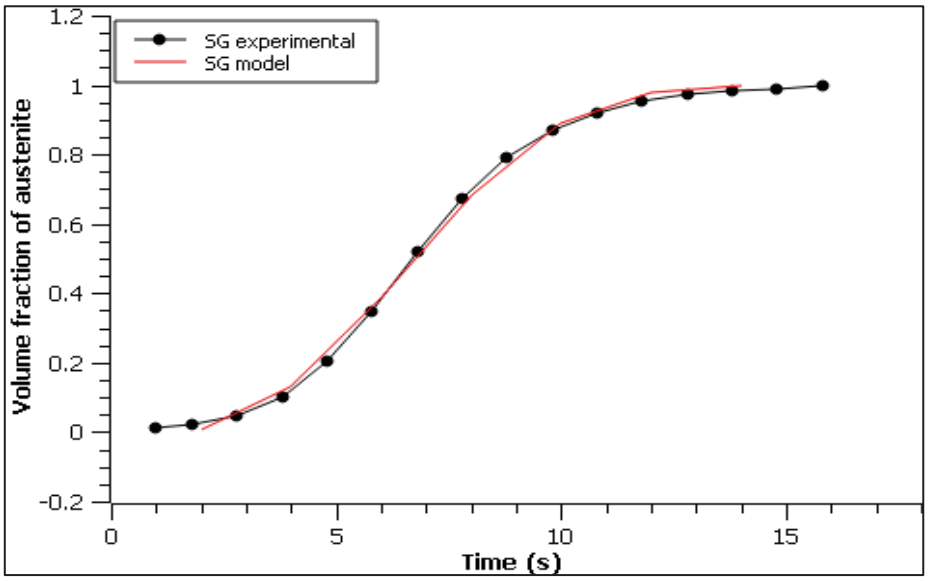

(a)

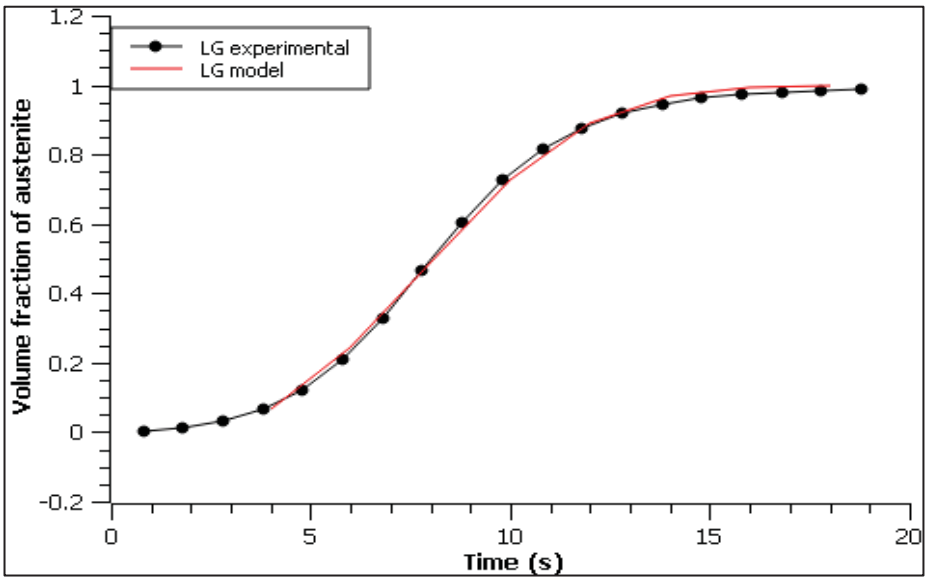

(b)

Figure 3.10 Comparison of modelled and measured kinetics of austenite formation for: (a) the SG sample and (b) the LG sample.

The mathematical model developed by Caballero et al. (Caballero et al., 2001) for ferrite to austenite phase transformation was effectively adapted in this study to examine the impact of initial grain size on martensite to austenite phase transformation. The frequency value of atomic jump ϑ, the enthalpy of activation per atom ΔH, the entropy of activation per atom ΔS were adjusted to account for the specific material used in this study. The Gibbs energy change per atom was calculated using Thermo-Calc and expressed as a quadratic function of temperature. The kinetic parameters A, B, and C in Eq. (3.10), representing nucleation at grain boundaries, grain edges, and grain corners, respectively, were modified for each grain size using the least squares optimization technique with a genetic algorithm solver.

3.4 Conclusions

In the present work, the influence of PAGS on the kinetics of austenite formation has been investigated for a medium-carbon low-alloy steel. The following conclusions can be drawn:

1- The kinetics of austenite formation from an initial martensite microstructure increases with a decrease in PAGS.

2- The critical temperature Ac1 during heating is not affected by PAGS.

3- The nucleation sites for austenite formation are prior austenite grain boundaries for an initial martensite microstructure.

4- The mathematical modelling of the kinetics of austenite formation from an initial martensite microstructure was conducted, where the model provided the amount of austenite formed for a given time, heating rate, and prior austenite grain size.

This study identified the importance of the initial grain size on the kinetics of austenite formation by providing a mathematical model of the martensite-to-austenite transformation.

This research was conducted on two distinct prior austenite grain sizes, representative of the surface and core regions of large ingots. Subsequent studies could explore a more extensive range of PAGS. Findings of this result will help optimize the thermal processes of heat treatments of steels in the manufacturing industry.

CHAPTER 4

Influence of Initial Phase and Heating Rate on the Kinetics of Austenite Formation in Medium Carbon Low Alloy Steel

4.1 Introduction

The heat treatment of steels, principally the austenite formation process, is a critical step in determining the final microstructure and, consequently, the mechanical properties of components used in various industrial applications, such as turbine shafts, landing gear, and mold steels. As established in Chapter 3, precise control over these transformations is paramount.(Lévesque et al., 2020). While extensive research has focused on phase transformations during cooling, recent advancements in high-strength steels have emphasized the importance of understanding microstructural changes during heating, specifically the formation of austenite. The preceding literature review, summarized in this section, was essential for identifying the specific knowledge gaps regarding the influence of the initial phase (bainite and martensite) and heating rate on austenite formation kinetics. This knowledge then guided the development of the experimental plan and the final mathematical model presented in this chapter.

The initial microstructure of steel significantly influences the kinetics of austenite formation. Dannoshita et al. (Dannoshita et al., 2019) investigated the impact of initial ferrite-pearlite, bainite, and martensite phases on austenite formation in a low-carbon steel during inter-critical annealing. Their findings indicated that the kinetics of austenite formation varied considerably with the initial phase, with ferrite-pearlite showing faster kinetics than bainite, and martensite exhibiting the slowest kinetics at 7°C°C. This highlights the distinct behavior of different starting phases. Law and Edmonds (Law & Edmonds, 1980) also noted that austenite nucleation in martensitic and bainitic structures tends to be concentrated at prior austenite grain boundaries, with some intragranular nucleation. They observed that acicular austenite, which

inherits the lath structure, is favored by low austenitizing temperatures, while higher temperatures promote a more globular morphology. Interestingly, they found that retained austenite films in martensite were not detected at austenitizing temperatures, suggesting their rapid decomposition upon heating (Law & Edmonds, 1980).

In the context of bainitic microstructures, Yang and Bhadeshia (Yang & Bhadeshia, 1989) investigated re-austenitization from bainitic ferrite and acicular ferrite, finding that the transformation rate was slower for acicular ferrite due to a smaller austenite-ferrite interface area per unit volume. Caballero et al. (Caballero et al., 2005) studied high silicon bainitic steels and found that retained austenite often decomposes into ferrite and carbides upon heating before it can grow, thus requiring new austenite nucleation. Yang and Bhadeshia (Yang & Bhadeshia, 1991) further elaborated that at small heating rates, residual austenite in bainitic microstructures tends to decompose, leading to similar austenitization behavior as tempered bainite (which requires nucleation). However, at faster heating rates, residual austenite remains stable and can grow without prior nucleation. Yang and Huang (Yang & Huang, 1993) observed that in bainitic ferrite-austenite mixtures, the rate of austenite formation increased with increasing austenite formation temperature, and the degree of substitutional alloying element redistribution decreased at higher temperatures, indicating a dependence of the transformation mechanism on the driving force. Li et al. (D. Li et al., 2010)investigated austenite formation in a copper-bearing steel with an initial microstructure of ferrite and bainite, identifying two distinct stages: an initial diffusion-controlled dissolution of ferrite and most of the bainite, followed by a shear-controlled dissolution of the remaining bainite and austenite formation. This multi-stage process highlights the complexity of transformations from mixed initial microstructures. The differences in reaction rates and mechanisms between martensitic and bainitic starting microstructures are critical for precise heat treatment design.

Beyond the initial microstructure, the heating rate is another crucial parameter that dictates the kinetics of austenite formation and the critical transformation temperatures (A_{c1} and A_{c3}). Li et al. (D. Li et al., 2010) confirmed that critical temperatures for austenite formation increase with increasing heating rate, with a distinct effect on the A_{c1} temperature. They suggested that

the process is mainly controlled by diffusion when the heating rate exceeds 1 °C/s. Law and Edmonds (Law & Edmonds, 1980) observed that A_{c1} temperatures decreased as heating rates were reduced, and that for all heating rates, A_{c1} was lowest for martensite, followed by bainite, and then ferrite, qualitatively correlating with their observed nucleation rates. Andrade-Carozzo and Jacques (Andrade-Carozzo & Jacques, 2007) explored the complex interactions between ferrite recrystallization and austenite formation during annealing of cold-rolled Nb-added TRIP steels. They found that niobium addition retards ferrite recrystallization, leading to an overlap with austenite formation during fast heating. In such cases, unrecrystallized ferrite enhances austenite nucleation, which in turn hinders further recrystallization. They also highlighted that the heating rate influences the thermodynamic conditions at the ferrite/austenite interface: fast heating can lead to austenite formation under paraequilibrium conditions (resulting in a larger initial austenite fraction), while slow heating promotes local equilibrium conditions from the outset. This implies that the heating rate can significantly alter the balance and interplay between different microstructural transformations, thereby increasing the kinetic differences observed when starting from bainitic versus martensitic microstructures. For instance, a faster heating rate might push the transformation from martensite more towards a displacive mechanism, while a bainitic structure might still be dominated by diffusional processes, thus accentuating the kinetic disparity.

In recent years, significant advancements have been made in developing mathematical frameworks to analyze the thermal processes associated with austenite formation, integrating thermodynamics with microstructural changes. The objective of these models is to accurately predict the proportion of austenite and enhance precision in evaluating phase distribution within multiphase steels for microstructure design. Vasilyev et al. (Vasilyev et al., 2019) developed a quantitative mathematical model for austenitization kinetics and final austenite grain size under continuous heating, applicable to steels with initial microstructures including ferrite, pearlite, bainite, and martensite. Their model considers nucleation on cementite particles at various sites, such as pearlite colony edges, ferrite grain boundaries, and within bainite/martensite volumes, with growth rates determined by the specific initial microstructure component and heating rate. While this model demonstrates good agreement across a wide

range of conditions and confirms the importance of starting phase characteristics, such broad frameworks often focus on general phase transformations rather than the distinct comparative behavior between specific phases. Consequently, a gap remains in quantifying the precise kinetic disparities and sensitivities specifically between bainitic and martensitic initial microstructures in medium-carbon low-alloy steels.

The present study aims to build upon this foundation by investigating the combined effects of initial phase (bainite and martensite) and heating rate on the kinetics of austenite formation. While previous research has explored these factors individually or in specific contexts, a comprehensive understanding of their synergistic influence, in medium-carbon, low-alloy steels, remains crucial for optimizing heat treatment processes and predicting final material properties. The present work seeks to address this gap by providing a detailed analysis of how the initial bainitic and martensitic microstructures, coupled with varying heating rates, affect the transformation kinetics and mechanisms of austenite formation.

4.2 Materials and Methods

This section delineates the comprehensive experimental and characterization methodologies employed to investigate the intricate kinetics of austenite formation in a medium-carbon, low-alloy steel. Building upon the foundational understanding established in Chapter 3 regarding the influence of prior austenite grain size on martensite-to-austenite transformation, the present work extends this inquiry to explore the combined effects of initial microstructure (specifically martensite and bainite) and varying heating rates on the austenite formation process.

The material utilized for this investigation was a medium-carbon, low-alloy steel, supplied by Finkl Steel-Sorel, Quebec, Canada, with its nominal chemical composition consistent with the details provided in Chapter 3. Cylindrical samples, precisely machined to 10 mm in length and 4 mm in diameter, served as the specimens for all dilatometric experiments. All thermal treatments, from initial microstructure preparation to continuous heating and intermittent

quenching, were meticulously executed using a Bahr 805D/A high-resolution dilatometer (TA Instruments, New Castle, DE, USA), which afforded precise control over the thermal cycles. To establish the distinct initial microstructures critical for this study, samples underwent specific thermal processing protocols shown in Figure 4.1. For the martensitic initial microstructure, characterized by a consistent prior austenite grain size (PAGS) of approximately 117 μm, samples were initially heated to 1100 °C at a rate of 5 °C/s. This was succeeded by an isothermal hold for 5 minutes, followed by rapid cooling at 10 °C/s using helium gas to ensure a complete martensitic transformation. Concurrently, bainitic initial microstructures, also exhibiting a PAGS of approximately 117 μm, were prepared. This involved heating samples to 1100 °C at a rate of 5 °C/s, holding for 5 minutes, and then a controlled cooling rate of 0.08 °C/s using Argon gas to achieve the desired predominantly bainitic structure. The parameters used for preparing the initial microstructure were adopted from the literature concerning medium carbon low alloy steel (Talebi et al., 2018)

After the preparation of these well-defined initial microstructures, continuous heating experiments were systematically conducted to probe the kinetics of austenite formation. Samples, encompassing both martensitic and bainitic starting conditions, were heated from room temperature at precisely controlled rates of 0.5 °C/s, 5 °C/s, and 25 °C/s. These rates were specifically chosen to simulate distinct industrial thermal cycles: 0.5 °C/s reflects the slow heating experienced at the center of a large forged ingot; 5 °C/ represents the faster heating typical of the ingot surface; and 25 °C/s models the very rapid localized heating associated with processes like ingot crack repair. The dilatometric curves, which meticulously record the change in sample length as a function of temperature, were rigorously analyzed. This analysis facilitated the precise determination of critical transformation temperatures, namely the austenite start (A_{c1}) and finish (A_{c3}) temperatures. The evolving volume fraction of austenite throughout the heating process was quantitatively calculated from the dilatometric data using the established lever rule.

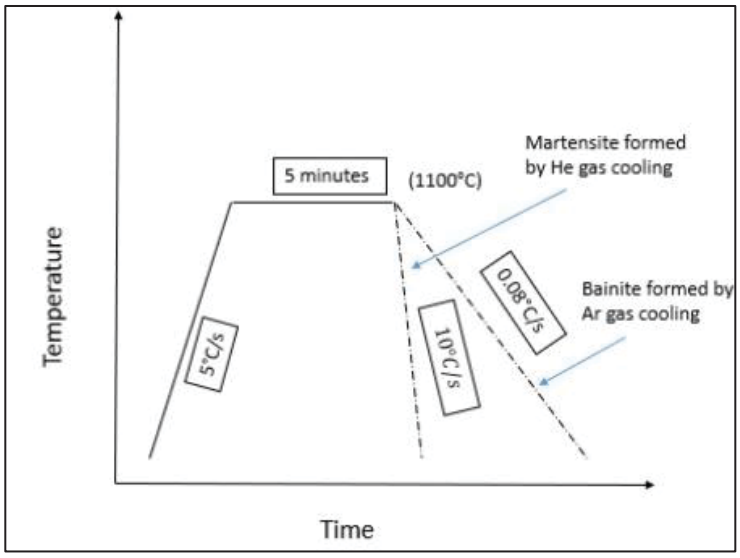

Figure 4.1 Schematic of the Thermal Processing Cycles used to establish the distinct initial microstructures

To delve deeper into the fundamental nucleation and growth mechanisms governing austenite formation, a series of intermittent quenching tests were performed. In these specialized experiments, samples were heated at a rate of 5 °C/s to temperature just above A_{c1} to 780 °C. Upon reaching this pre-determined temperature, samples were immediately quenched using a high-velocity helium gas stream at a rapid cooling rate of 40 °C/s. This swift quenching effectively preserved the high-temperature austenite, transforming it into martensite at ambient temperature, thereby facilitating subsequent microstructural examination of the austenite's morphology and spatial distribution at various stages of transformation.

Comprehensive microstructural characterization was integral to this study, employing a suite of advanced techniques to corroborate dilatometric findings and elucidate microstructural evolution. Samples designated for microstructural observation underwent meticulous preparation, adhering to standard metallographic procedures including grinding and polishing. For conventional optical microscopy, a 3% Nital etchant was applied to reveal general microstructural features. To accurately quantify the Prior Austenite Grain Size (PAGS), a technique challenging in martensitic structures where conventional chemical etching is often ineffective, a thermal etching method was utilized. This involved heating polished samples in an inert atmosphere, which induced the formation of subtle grooves along the prior austenite

grain boundaries, making them discernible under an optical microscope. A Laser Confocal Microscope LEXT4100 (Olympus, Tokyo, Japan) was employed for detailed optical examination of the etched microstructures and for measuring PAGS in accordance with the ASTM E-112 standard method. For higher-resolution analysis of nucleation sites and the precise distribution of phases following intermittent quenching, a SU8230 Hitachi Field-Emission Gun Scanning Electron Microscope (Hitachi, Tokyo, Japan) was used, equipped with a Bruker FlatQuad detector for Electron Backscatter Diffraction (EBSD). Samples prepared for EBSD analysis underwent an additional critical step of ion milling on a Hitachi IM4000-plus ion miller machine (Hitachi, Tokyo, Japan) to ensure a clean, strain-free surface. EBSD data was systematically acquired at an operating voltage of 25 kV, a working distance of 18 mm, and a step size of 0.16 μm, with subsequent data processing performed using Bruker ESPRIT 2.2 software.

4.3 Results and Discussion

This section presents the experimental results concerning the kinetics of austenite formation in a medium-carbon, low-alloy steel, focusing on the influence of initial microstructure (specifically martensite versus bainite) and varying heating rates. The discussion meticulously integrates data obtained from dilatometric measurements, detailed microstructural observations, and the insights derived from the developed mathematical model to comprehensively elucidate the underlying transformation mechanisms. This integrated approach allows for a holistic understanding of how these critical parameters govern the complex process of austenite formation.

4.3.1 Initial Microstructure

The initial microstructures, namely martensite and bainite, were meticulously prepared as described in section 4.2. A sequential characterization approach was employed: first, Optical Microscopy was used to observe the microstructural morphology. This was followed by

comprehensive analysis using Scanning Electron Microscopy and Electron Backscatter Diffraction to definitively determine the precise phase constitution and internal crystallographic substructure prior to the commencement of the heating experiments. Initially, optical micrographs of the as-prepared martensitic and bainitic samples are presented in Figure 4.2 and Figure 4.3, providing a crucial preliminary microscopic view. These images vividly highlight the distinct morphological characteristics of each phase, allowing for an immediate visual differentiation. The martensitic microstructure typically exhibited a very fine, acicular lath morphology, which is inherently indicative of its shear-dominated formation process and the high internal energy stored within its lattice. In stark contrast, the bainitic microstructure displayed more globular or granular features, appearing visibly less acicular than the martensite, directly reflecting its different formation mechanism that involves a combination of both shear and diffusion. These initial optical observations were therefore essential for visually distinguishing and confirming the starting microstructural conditions before embarking on more detailed quantitative analysis.

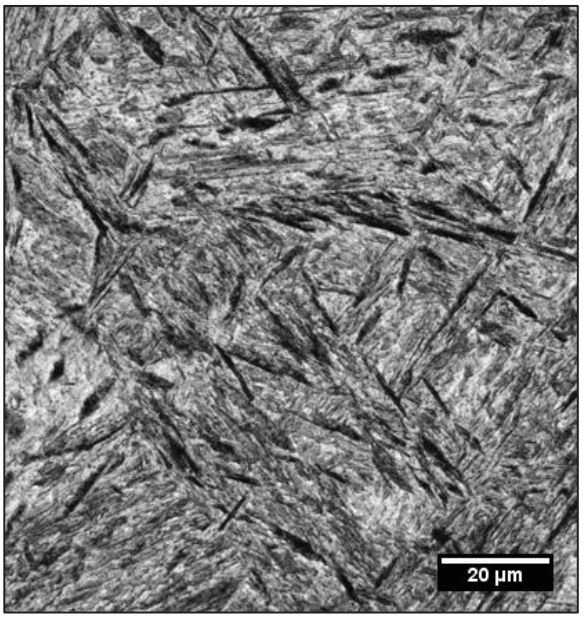

Figure 4.2 Optical micrograph of the initial martensite showing elongated, needle-like lath microstructure

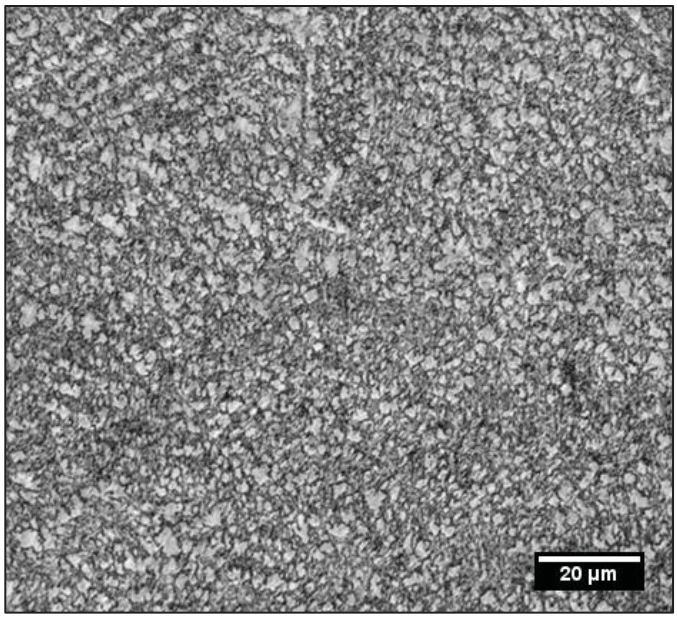

Figure 4.3 Optical micrograph of the initial bainite showing granular morphology

Following this initial optical examination, which revealed two distinct non-equilibrium morphologies, highly elongated, needle-like laths (characteristic of martensite or acicular bainite) and granular islands (characteristic of granular bainite) EBSD was utilized extensively. This was necessary because Optical Microscopy cannot definitively distinguish between these visually similar phases or provide the detailed crystallographic information required to analyze the precise phase constitution and intricate internal substructure. For the martensitic samples, the EBSD phase map (Figure 4.4) clearly confirmed a near 100% martensitic microstructure. The phase map, which assigns a specific color to each identified crystal structure, indicated the presence of regions with a Body-Centered Tetragonal or Body-Centered Cubic structure, which is the crystal structure of lath martensite, and these regions were geometrically arranged into packets composed of numerous laths, the typical defining morphology of lath martensite. This phase was characterized by its lath morphology, 11:00 amand the inherently high internal lattice strain a direct result of the austenite-to-martensite shear transformation that causes a localized volume change and accumulation of defects. This high internal strain is clearly visualized in the Image Quality (IQ) map, which is a grayscale representation of the sharpness and clarity of the Kikuchi diffraction patterns used to map the sample, where dark areas indicate highly strained or defective regions (low IQ). The phase map's distinct and accurate

identification of the martensitic regions throughout the sample validates the exceptional effectiveness of the quenching process in achieving the desired starting phase.

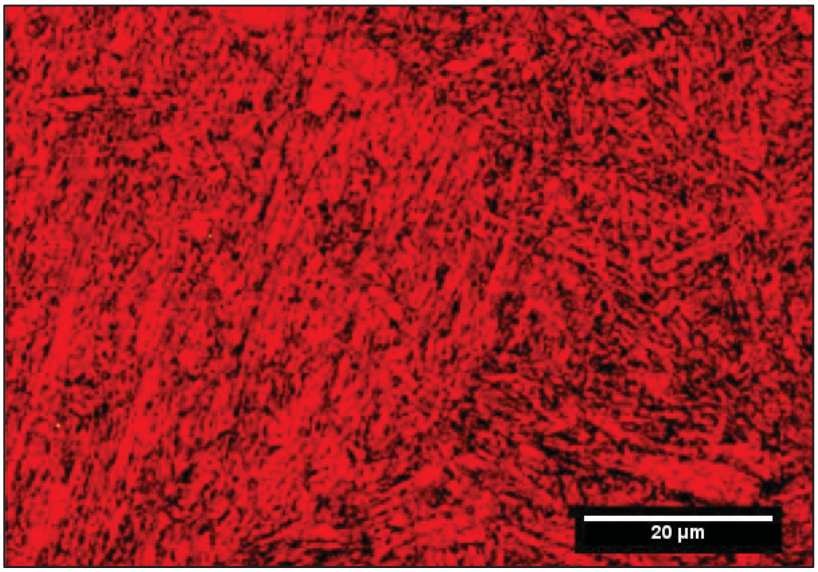

Figure 4.4 EBSD Phase Map of the initial martensitic microstructure showing near 100% transformation (BCT/BCC) phase.

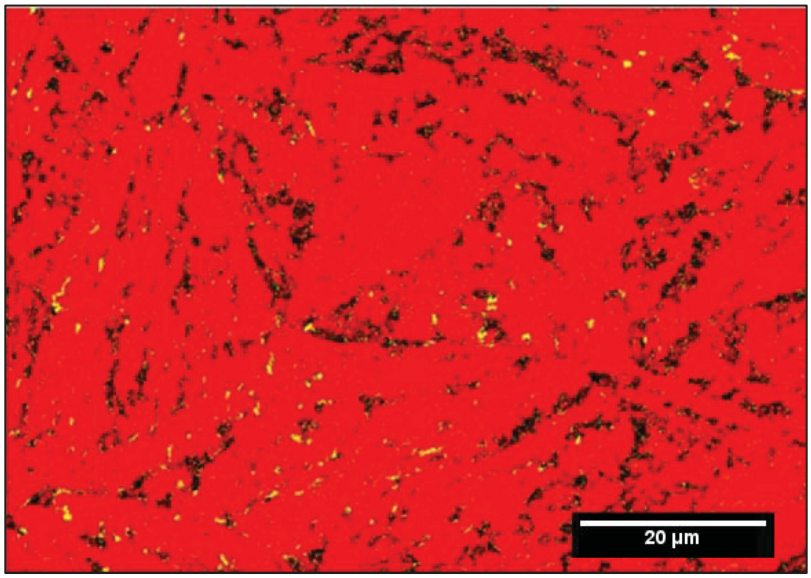

Figure 4.5 EBSD Phase Map of the bainitic microstructure, confirming a full transformation to bainite (BCC phase) and the absence of untransformed austenite.

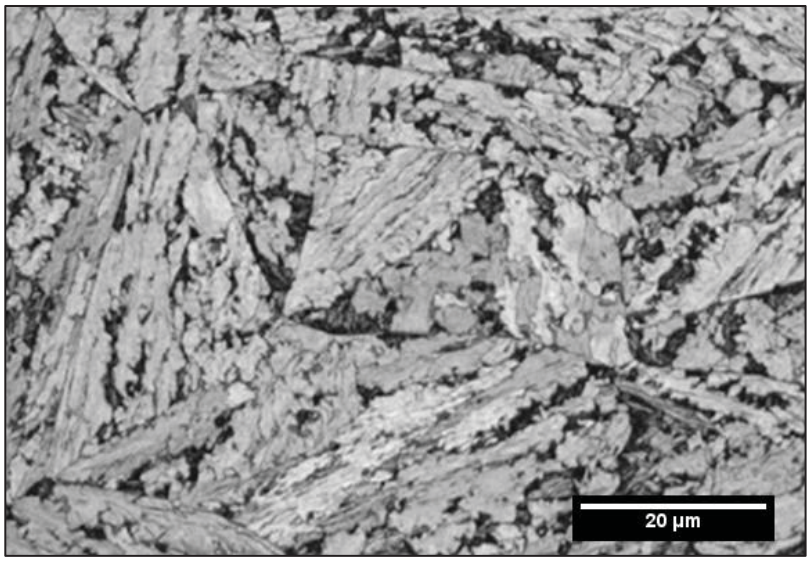

Figure 4.6 EBSD Image Quality Map of the bainitic microstructure, showing generally bright regions corresponding to high IQ.

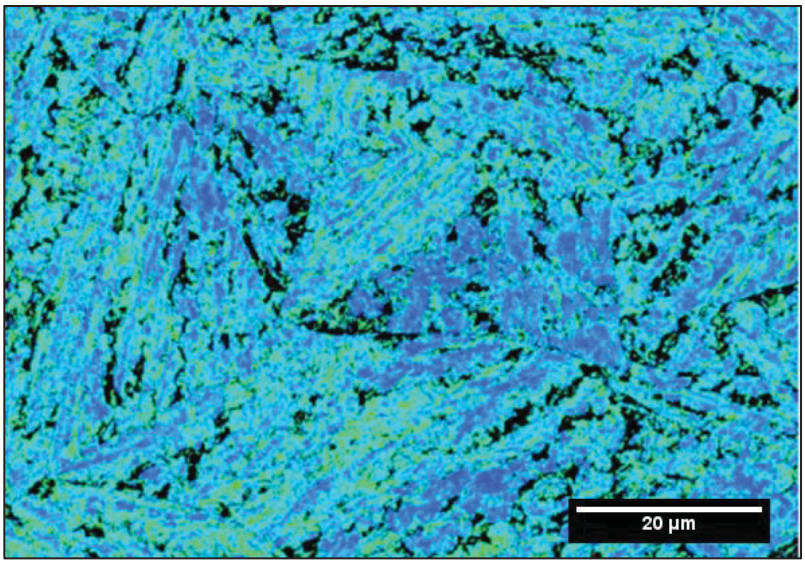

Figure 4.7 EBSD Kernel Average Misorientation Map for the bainite sample showing low internal misorientation, typically indicated by blue/dark colors.

For the bainitic samples, The EBSD phase map (Figure 4.5) and image quality map (Figure 4.6) conclusively demonstrated a fully bainitic microstructure with no discernible traces of other phases. The phase map, which assigns a specific color to each identified crystal structure, confirmed the complete absence of any untransformed austenite or other undesirable constituents, explicitly verifying the successful and complete transformation to bainite. Kernel

Average Misorientation (KAM) maps, obtained from the EBSD analysis (Figure 4.7), were utilized to precisely assess the internal misorientation within the bainitic laths. The KAM map measures the average misorientation between a point and its immediate neighbors, thus serving as a qualitative indicator of local strain or stored energy. The consistently low KAM values observed across the bainitic microstructure provided strong evidence of a complete bainitic transformation characterized by minimal internal lattice strain (as opposed to the high internal strain of martensite), thereby distinctly differentiating it from a martensitic structure which, owing to its displacive nature, typically exhibits significantly higher internal misorientation. This characterization ensured that the starting microstructures for all subsequent kinetic studies were homogeneous and consistent.

4.3.2 Critical Transformation Temperatures

The dilatometric analysis of continuous heating experiments provided precise measurements of the critical transformation temperatures, namely the austenite start (A_{c1}) and finish (A_{c3}) temperatures, for both martensitic and bainitic initial microstructures across the entire range of heating rates investigated. As illustrated in Figure 4.8, a clear and consistent distinction in critical temperatures was observed between the two initial phases. Specifically, the austenite start temperature (A_{c1}) for the bainitic microstructure was found to be consistently lower than that for the martensitic microstructure across all heating rates applied. This significant finding clearly indicates that, under the same heating conditions, austenite formation commences at a lower thermal threshold when the starting phase is bainite as compared to martensite. Such observations regarding the influence of the initial microstructure on critical transformation temperatures reported in the broader metallurgical literature (Law & Edmonds, 1980; Li et al., 2010), reinforcing the validity of our findings for bainite and martensite initial microstructure.

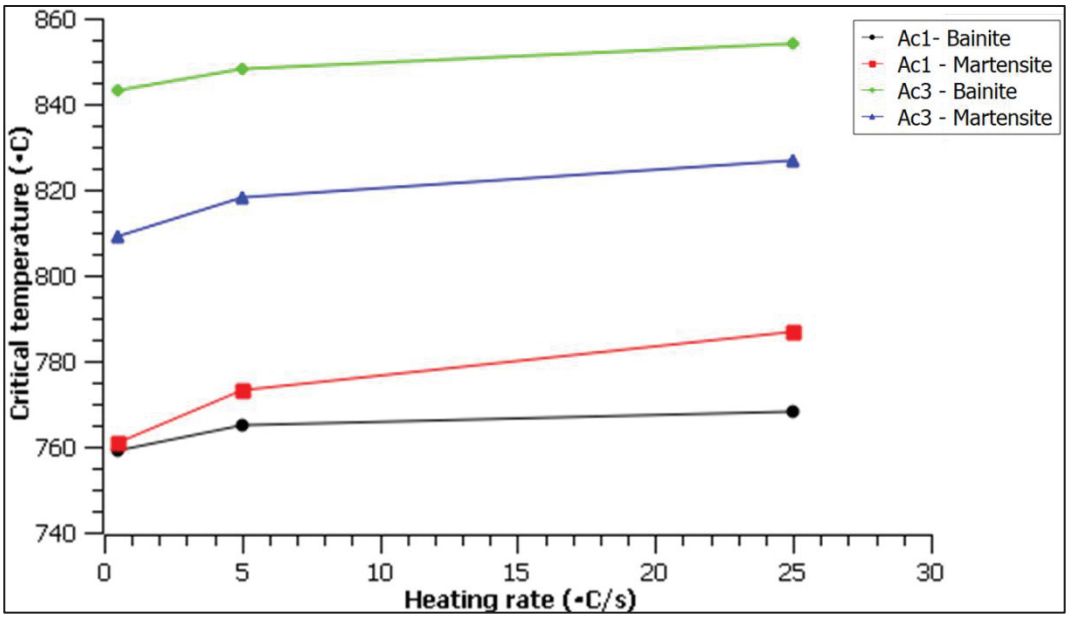

Figure 4.8 Change in critical temperatures with heating rate

A consistent and expected trend observed was that increasing the heating rate invariably led to an elevation of both the A_{c1} and A_{c3} temperatures for both microstructures. This upward shift in transformation temperatures is primarily attributed to the kinetic delay inherent in transformation processes at faster heating rates. Essentially, higher temperatures are required to provide the necessary thermal energy and sufficient driving force for the transformation to both initiate and proceed to completion within the shorter timeframes associated with rapid heating (D. Li et al., 2010; Vasilyev et al., 2019). Importantly, the impact of the heating rate on these critical temperatures was more striking for the bainitic samples than for the martensitic samples. This differential sensitivity strongly suggests that the bainitic microstructure is inherently more responsive and sensitive to changes in heating rate in terms of its transformation onset and completion temperatures, potentially implying distinct rate-controlling steps or varying activation energies governing the transformation in each initial phase.

4.3.3 Kinetics of Austenite Formation

The kinetics of austenite formation, quantitatively represented by the evolving volume fraction of austenite as a function of both time and temperature, exhibited remarkably significant

differences when comparing the martensitic and bainitic initial microstructures. As depicted in Figure 4.9, the martensitic microstructure consistently demonstrated a substantially faster austenite formation kinetics compared to the bainitic microstructure. This accelerated transformation in martensite is unambiguously evident from the steeper slope of its austenite volume fraction curve, which directly signifies a more rapid overall transformation rate. This substantial difference highlights the critical influence that the starting phase exerts on the reverse transformation to austenite, a phenomenon that has been reported for ferrite based initial microstructure (Dannoshita et al., 2019; Yang & Bhadeshia, 1989; Li et al., 2010) but not for bainitic and martensitic ones. This observed disparity in kinetics constitutes is one of the key and fundamental finding of this project.

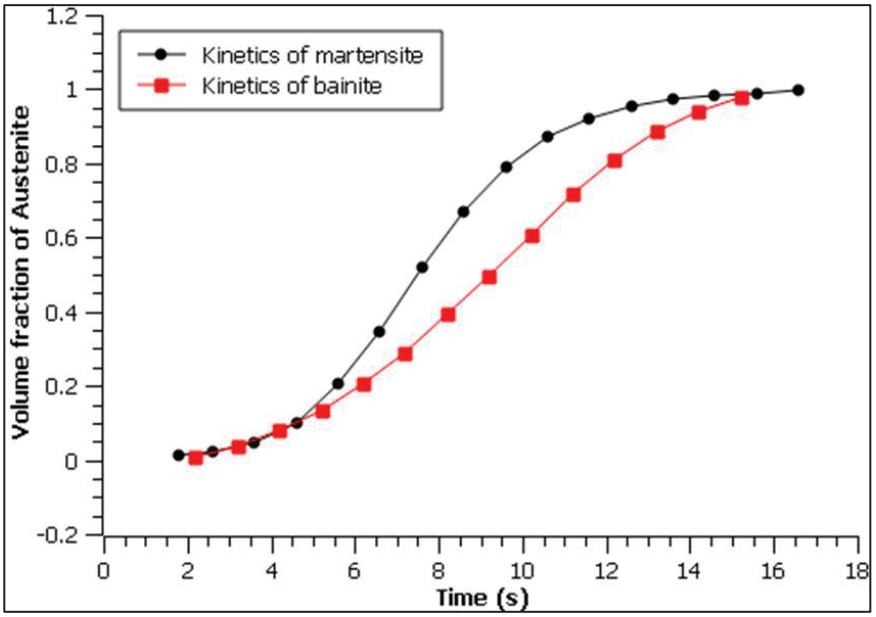

Figure 4.9 Kinetics of austenite formation for martensite vs bainite

The more rapid kinetics observed in martensite can be primarily attributed to its inherently higher stored energy and its extremely fine, highly dislocated substructure (Nishiyama, 2012). This unique internal state provides a significantly greater density of potential nucleation sites and considerably shorter diffusion paths for atomic rearrangement, especially when compared to the relatively coarser and less strained bainitic structure. The disparity in kinetics between

these two initial microstructures was further accentuated and became much clearer with increasing heating rates, as reported in Figure 4.9. This observation strongly suggests that as the thermodynamic system is driven further from equilibrium by the application of faster heating rates, the inherent differences in the fundamental transformation mechanisms and the available driving forces between martensite and bainite become increasingly prominent. This leads to a greater divergence in their overall transformation behavior, aligning well with broader observations by other researchers (Andrade-Carozzo & Jacques, 2007), who noted that heating rate can significantly alter the thermodynamic conditions and the resulting transformation behavior in materials with different initial microstructures.

4.3.4 Nucleation and Growth Mechanisms

Microstructural observations, derived from intermittent quenching tests (see Figure 4.10 and Figure 4.11), provided invaluable insights into the fundamental nucleation and growth mechanisms governing austenite formation in both microstructures. For both the martensitic and bainitic initial microstructures, it was consistently observed that austenite nucleation preferentially occurred at the prior austenite grain boundaries (PAGBs). This strong preference indicates that PAGBs serve as exceptionally potent heterogeneous nucleation sites for the reverse transformation, most likely due to their inherently high energy, numerous structural irregularities, and increased atomic mobility (Law & Edmonds, 1980; Caballero et al., 2005). These boundaries offer energetically favorable locations for the initial formation of austenite nuclei. As seen in Figure 4.10 and Figure 4.11, the prior austenite grain size (PAGS) for both samples is approximately 117 μm. This PAGS was determined by thermal etching, the details of which were mentioned in Chapter 3. This PAGS is comparable to the PAGS typically found near the surface of large industrial ingots.

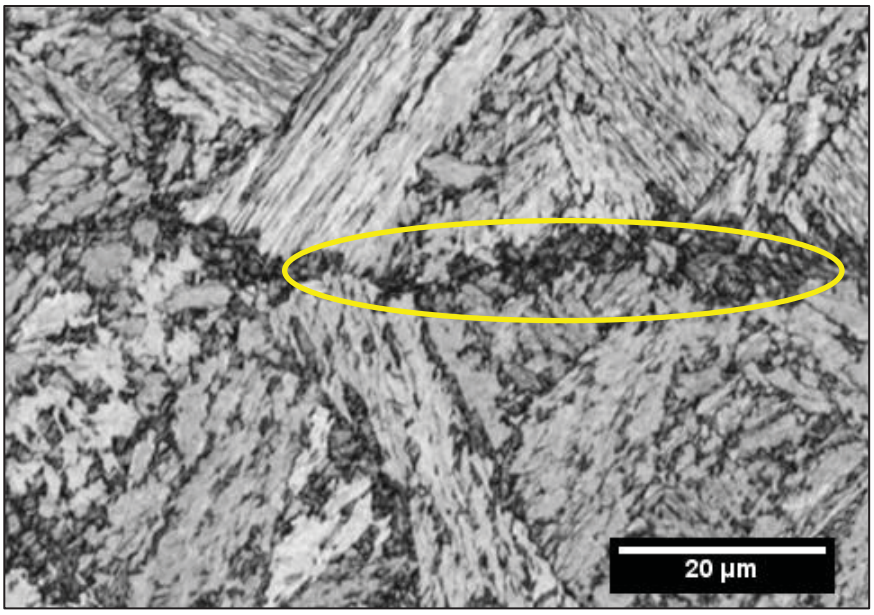

Figure 4.10 Image quality map showing grain boundary nucleation in martensite sample

While the primary nucleation sites appeared to be similar for both initial microstructures, the observed difference in the overall growth rates between martensite and bainite is hypothesized to stem significantly from variations in carbon distribution within their respective matrices. Martensite, being a highly supersaturated solid solution of carbon in ferrite, inherently offers a more uniform and readily available supply of carbon for the growth of austenite. This contrasts with bainite, which involves some degree of carbon partitioning during its formation, potentially leading to a less uniform carbon distribution or the presence of carbides that require dissolution (Yang & Huang, 1993). This fundamental difference in local carbon concentration and its distribution could influence the local equilibrium conditions at the advancing austenite/matrix interface, thereby directly affecting the growth kinetics.

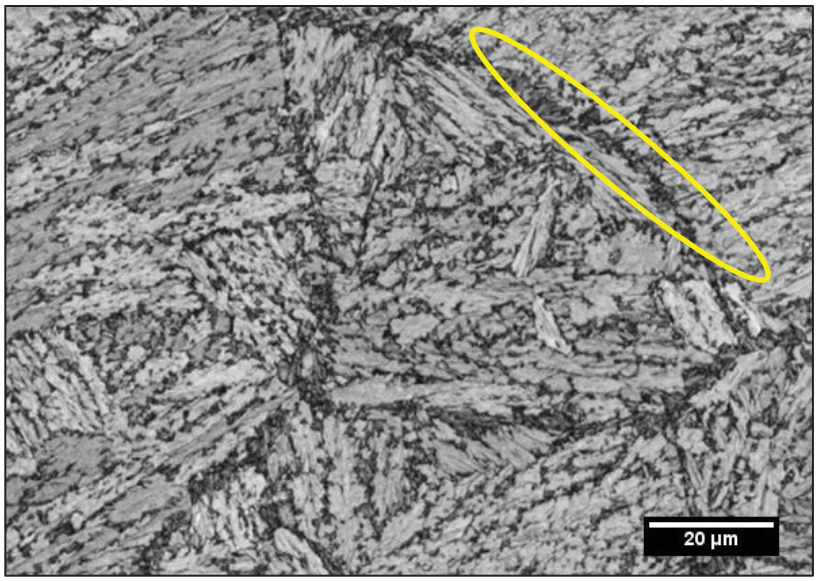

Figure 4.11 Image quality map showing preferential nucleation at prior austenite grain boundary for bainite

4.3.5 Mathematical Modeling of Austenite Formation Kinetics

A comprehensive mathematical model was meticulously developed to quantitatively describe the kinetics of austenite formation from the bainitic initial microstructure, critically incorporating the influence of heating rate as a key variable. This modeling effort builds directly upon the fundamental framework utilized for the martensite-to-austenite transformation discussed in Chapter 3. As detailed in Chapter 3, the determination of the kinetic parameters for the martensitic microstructure, specifically the coefficients A1, A2, and A3, was achieved through a rigorous optimization process utilizing the Least Squares Technique (LST) in conjunction with a Genetic Algorithm (GA). Given that the nucleation pattern for austenite formation from bainite was also observed to occur predominantly at prior austenite grain boundaries (PAGBs), like that in martensite, the core mathematical model structure was adapted. This approach allowed for consistency in the theoretical basis while accounting for the distinct characteristics of the bainitic matrix.

The objective function for this optimization was defined as minimizing the sum of the squared differences between the experimentally measured austenite volume fractions and those

predicted by the mathematical model. The Genetic Algorithm, a versatile optimization solver, was employed due to its effectiveness in exploring complex, non-linear, and potentially discontinuous design spaces, which is characteristic of microstructural transformation problems. The GA iteratively refined the values of A1, A2, and A3 by simulating natural selection processes, including population generation, selection of fitter individuals, crossover, and mutation, until an optimal fit to the experimental dilatometry data was achieved. This optimization ensured that the derived coefficients precisely reflect the unique nucleation and growth characteristics of austenite formation from the bainitic microstructure.

As summarized in Table 4.1, kinetic parameters were derived and obtained for the bainitic microstructure, reflecting its individual transformation characteristics. The coefficients of activated growth sites (A1, A2, A3), which represent the contributions of nucleation and growth from different geometric features (such as grain boundary edges, faces, and corners), were found to differ significantly from those for martensite. This divergence is attributed to the inherently slower overall kinetics of bainite (as discussed in Section 3.3), which is influenced by its distinct carbon distribution (carbon partitioning and carbide presence, as noted in Section 3.4) affecting local growth rates and interface mobilities. Similarly, the enthalpy of activation per atom (ΔH) shown in Table 4.2, representing the energy barrier for atomic transfer across the interface, was precisely determined for bainite. This value is distinct from that of martensite, reflecting the different nature of the bainitic matrix (bainitic ferrite and associated carbides) and the energy required for atomic movement across the bainite/austenite interface. The greater sensitivity of bainite to the applied heating rate, as highlighted in Section 3.2, further implies differing energy barriers and rate-controlling steps. The model predicted the experimental kinetics for bainite with a strong agreement between the simulated and measured transformation curves as shown in Figure 4.12. This validation confirms the model's capability to capture the complex interplay between the bainitic initial microstructure and the applied heating rate on austenite formation kinetics, aligning well with advanced modeling approaches that account for various microstructural components and thermal conditions (Vasilyev et al., 2019).

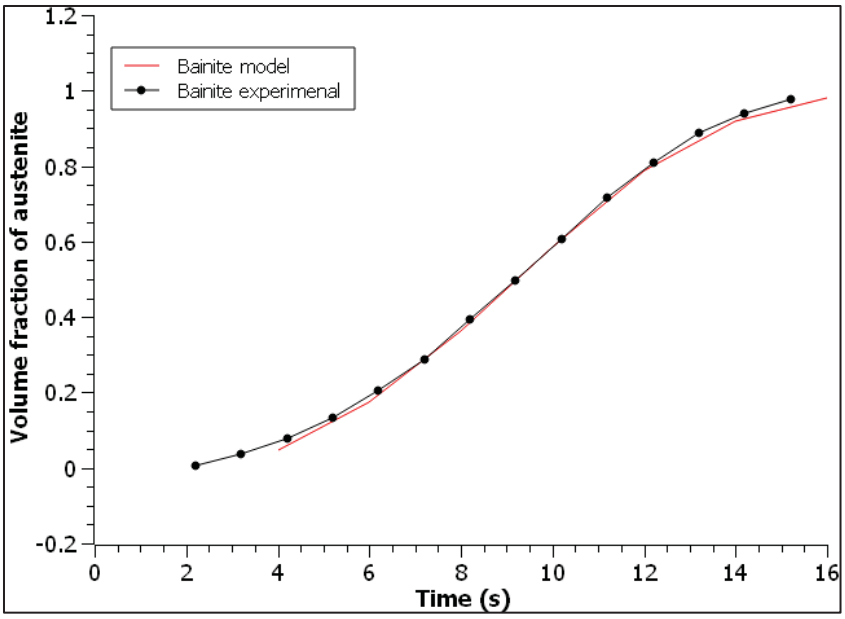

Figure 4.12 Comparison of modelled and measured kinetics of austenite formations for the initial bainite microstructure that is heated at 5°C/s

Table 4.1 Coefficients of activated growths between martensite and bainite

Samples	Coefficients of activated growth		
	A1	A2	A3
Martensite	0.48	13.30	4
Bainite	0.09	13.13	4.36

Table 4.2 Change in enthalpy between martensite and bainite

Samples	ΔH/ atom (J/atom)
Martensite	240.3×10^{-21}
Bainite	245.3×10^{-21}

4.4 Summary

In summary, the comprehensive investigation conducted in this study has revealed several critical and impactful aspects concerning the kinetics of austenite formation in the medium-

carbon, low-alloy steel. Firstly, it was consistently observed that preferential nucleation sites for austenite formation in both martensitic and bainitic initial microstructures are the prior austenite grain boundaries, highlighting their critical role in initiating the transformation. Secondly, a clear and highly significant difference in austenite formation kinetics exists between martensitic and bainitic starting microstructures, with the martensitic phase consistently transforming at a faster rate. This kinetic disparity highlights the profound influence of the starting microstructure on the reverse transformation behavior.

Thirdly, the heating rate was found to exert a substantial impact on both the critical transformation temperatures and the overall transformation kinetics. Notably, a stronger effect of heating rate was observed for the bainitic microstructure, indicating its greater sensitivity to thermal cycling. This differential response to heating rate also serves to increase the inherent difference in kinetics observed between starting microstructures of bainite and martensite, making their transformation pathways diverge more significantly at higher heating rates. The developed mathematical model quantifies the austenite formation kinetics for both initial microstructures with high accuracy, thereby providing a predictive tool for understanding and controlling transformation behavior under varying thermal conditions. These collective findings contribute significantly to the fundamental understanding of phase transformations and offer valuable insights for optimizing heat treatment processes in the manufacturing industry, chiefly for high-value-added steel components where precise microstructural control is paramount.

CONCLUSION

The mechanical properties and performance of medium-carbon low-alloy steels, essential for critical components such as aircraft landing gear and hydraulic turbines, are dictated by precise control over their phase transformations during thermal processing. This thesis addressed significant knowledge gaps regarding the non-isothermal formation kinetics of austenite from complex, non-equilibrium initial microstructures, martensite and bainite, and the synergistic roles of prior austenite grain size (PAGS) and heating rate. By employing high-resolution dilatometry, advanced microstructural characterization (SEM/EBSD), and mathematical modeling, this research has established a comprehensive framework for understanding and predicting these vital transformation behaviors.

A major contribution of this work lies in quantifying the impact of PAGS on the kinetics of martensite-to-austenite transformation. It was definitively demonstrated that grain refinement, specifically a reduction in PAGS from 330 μm (representing the core of a forged ingot) to 117 μm (representing the surface), leads to a significant acceleration in the austenite formation rate. This effect is attributed to the increased density of potent Prior Austenite Grain Boundaries (PAGBs), which were unequivocally identified as the primary nucleation sites for the new austenite phase. This difference in PAGS was found to influence the transformation kinetics without altering the critical austenite start temperature (A_{c1}).

Further comparative analysis revealed a fundamental kinetic divergence between the two non-equilibrium starting phases. The martensitic microstructure exhibited substantially faster overall austenite formation kinetics than the bainitic microstructure under identical continuous heating conditions. This kinetic disparity is a direct consequence of the intrinsic differences in their internal energy states and carbon distributions. The rapid transformation in martensite is driven by its highly strained, carbon-supersaturated lattice, offering readily available carbon for austenite growth. The innately slower kinetics observed in bainite are hypothesized to stem from the need to dissolve or bypass pre-existing carbides formed by carbon partitioning during its formation, leading to distinct rate-controlling steps.

The research quantified the pervasive influence of the heating rate on the transformation process. Increasing the heating rate consistently elevated the critical temperatures for both microstructures due to kinetic retardation. However, the bainitic microstructure exhibited higher sensitivity to the heating rate, suggesting that differing activation energies govern the atomic transfer across the interface compared to martensite. As heating rates increase, this distinct response further emphasizes and measures the difference in transformation kinetics between initial martensite and initial bainite microstructure, offering a definitive benchmark for how these two non-equilibrium phases diverge.

Further comparative analysis revealed a fundamental kinetic divergence between the two non-equilibrium starting phases. The martensitic microstructure exhibited substantially faster overall austenite formation kinetics than the bainitic microstructure under identical continuous heating conditions. This kinetic disparity is a direct consequence of the intrinsic differences in their internal energy states and carbon distributions. The rapid transformation in martensite is fuelled by its highly strained, carbon-supersaturated lattice, offering readily available carbon for austenite growth. The slower kinetics observed in bainite are hypothesised to stem from the need to dissolve or bypass pre-existing carbides formed by carbon partitioning during its formation, leading to distinct rate-controlling steps.

The research quantified the influence of the heating rate on the transformation process. Increasing the heating rate consistently elevated both the A_{c1} and A_{c3} temperatures for both microstructures due to kinetic retardation. However, the bainitic microstructure exhibited a stronger sensitivity to the heating rate, suggesting differing activation energies govern the atomic transfer across the interface compared to martensite. This differential response further accentuates the gap in transformation kinetics between martensite and bainite as the heating rate increases.

A final, integral achievement of this thesis was the development and validation of mathematical models rooted in diffusion-controlled nucleation and growth theories. By adapting and optimizing these models using a Genetic Algorithm based on extensive

experimental dilatometry data, we created a predictive tool capable of quantifying the extent of austenite formation as a function of time, heating rate, initial microstructure, and PAGS (for martensite). The exceptional agreement demonstrated between the modeled predictions and the experimental results ($R^2 = 0.99$) validates the assumptions and provides a high-fidelity tool for process engineers.

In summary, this research provides vital, quantitative insights into the fundamental metallurgy of medium-carbon low-alloy steels. The findings concerning PAGS and the distinct kinetic behaviors of martensite and bainite are critical for optimizing industrial heat treatment schedules. The derived predictive mathematical models offer manufacturers the capability to design precise thermal processing routes, enabling exact microstructural control, minimizing energy consumption, and ensuring the final component properties meet stringent operational demands. This work represents a significant step forward in translating fundamental phase transformation knowledge into practical, industrial process optimization. The systematic characterization and modeling presented herein substantially enhance the fundamental understanding of non-equilibrium phase transformation kinetics, offering a sturdy foundation for the continued development of high-performance steel alloys.

RECOMMENDATIONS

This doctoral research has provided a quantitative and predictive framework for understanding the non-isothermal kinetics of austenite formation in a medium-carbon low-alloy steel. While the study addressed the influence of prior austenite grain size (PAGS) and the comparative transformation behavior of martensite and bainite, the findings open several promising avenues for future research to further refine the predictive models and expand the industrial applicability of the results.

1. Expansion of Microstructural Parameters and Scope

The current study focused on two distinct PAGS values representative of industrial extremes (surface and core of a large ingot). Future work should systematically investigate the kinetics of martensite-to-austenite transformation across a wider, continuous range of PAGS values. This broader experimental dataset would allow for the development of a fully interpolated model, enabling engineers to predict kinetics for any intermediate grain size, significantly enhancing industrial control.

2. Mechanistic Validation of Bainite Kinetics

The hypothesis that the slower kinetics in the bainitic microstructure stem from carbon partitioning and the presence of carbides requires explicit, high-resolution validation. Future research should employ complementary, highly localized characterization techniques:

Atom Probe Tomography (APT): To directly map the localized carbon content in the bainitic ferrite, retained austenite films, and carbide precipitates, confirming the precise carbon distribution before and during the initial stages of heating.

Transmission Electron Microscopy (TEM): To analyze the morphology, size, and crystallographic orientation of carbides in the initial bainite, and track their dissolution kinetics

during non-isothermal heating, providing a direct mechanistic link to the observed sluggish transformation rate.

3. Advanced Mathematical Model Refinement and Generalization

The predictive models developed in this work show high fidelity for the tested conditions. To elevate them to a more generalized engineering tool, the following steps are recommended:

Integrate Compositional Effects: Extend the current models to incorporate the effects of key substitutional alloying elements (e.g., Mn, Cr), which can influence the A_{c1} temperature and the diffusion coefficients.

Modeling Retained Austenite: The current model focuses on the martensite/bainite to austenite transformation. Future models should explicitly incorporate the evolution and stability of retained austenite present in the initial microstructures, tracking its decomposition or growth upon heating, especially since its stability is highly dependent on the heating rate.

Model Validation at Higher Heating Rates: While heating rates up to 25 °C/s were investigated, industrial processes like induction heating can employ rates exceeding 100 °C/s. Validating the current model at these extreme rates is essential for extending its utility to high-speed manufacturing applications.

By pursuing these recommendations, the fundamental understanding and the industrial utility of the predictive models for phase transformation control in medium-carbon low-alloy steels will be significantly advanced.

BIBLIOGRAPHY

Akbay, T., Reed, R. C., & Atkinson, C. (1994). Modelling reaustenitisation from ferrite/cementite mixtures in FeC steels. *Acta Metallurgica Et Materialia*, *42*(4), 1469–1480. https://doi.org/10.1016/0956-7151(94)90165-1

Andrade-Carozzo, V., & Jacques, P. J. (2007). Interactions between recrystallisation and phase transformations during annealing of cold rolled Nb-added TRIP-aided steels. *Materials Science Forum*, *539–543*(PART 5), 4649–4654. https://doi.org/10.4028/www.scientific.net/msf.539-543.4649

Ben Fredj, E., Ghasemi Nanesa, H., Jahazi, M., & Morin, J. B. (2018). Influence of initial microstructure and grain size on transformation of bainite to austenite in large size forgings. *Journal of Iron and Steel Research International*, *25*(5), 554–562. https://doi.org/10.1007/s42243-018-0070-y

Bhadeshia, H. K. D. H. (2010). Phase transformations contributing to the properties of modern steels. *Bulletin of the Polish Academy of Sciences. Technical Sciences*, *Vol. 58*(nr 2), 255–265. https://doi.org/10.1179/17428409X433813

Bhadeshia, H. K. D. H. (2019). Bainite in Steels : Theory and Practice, Third Edition. *Bainite in Steels*. https://doi.org/10.1201/9781315096674

Caballero, F. G., Capdevila, C., & García de Andrés, C. (2001). Kinetics and dilatometric behaviour of non-isothermal ferrite-austenite transformation. *Materials Science and Technology*, *17*(9), 1114–1118. https://doi.org/10.1179/026708301101511031

Caballero, F. G., Garcı-Mateo, C., & García de Andrés, C. (2005). *Dilatometric Study of Reaustenitisation of High Silicon Bainitic Steels : Decomposition of Retained Austenite*. *46*(3), 581–586.

Cahn, J. W. (1956). The Kinetics of Grain Boundary Nucleated Reactions. *Acta Metallurgica*, *4*.

Callister, W. D. , Jr. , & Rethwisch, D. G. ,. (2018). *Materials Science and Engineering, An Introduction, 10th Edition*. 1–992.

Carlone, P., Palazzo, G. S., & Pasquino, R. (2010). Finite element analysis of the steel quenching process: Temperature field and solid–solid phase change. *Computers &*

Mathematics with Applications, *59*(1), 585–594. https://doi.org/10.1016/J.CAMWA.2009.06.006

Celada-Casero, C., Sietsma, J., & Santofimia, M. J. (2019). The role of the austenite grain size in the martensitic transformation in low carbon steels. *Materials and Design*, *167*. https://doi.org/10.1016/j.matdes.2019.107625

Chipman, J. (1972). Thermodynamics and phase diagram of the Fe-C system. *Metallurgical Transactions*, *3*(1), 55–64. https://doi.org/10.1007/BF02680585

Christian, J. W. (2002). The Theory of Transformations in Metals and Alloys. *Pergamon Press, Oxford*. https://doi.org/10.1016/B978-0-08-044019-4.X5000-4

Dannoshita, H., Ogawa, T., Maruoka, K., & Ushioda, K. (2019). Effect of initial microstructures on austenite formation behavior during intercritical annealing in low-carbon steel. *Zairyo/Journal of the Society of Materials Science, Japan*, *68*(9), 718–722. https://doi.org/10.2472/jsms.68.718

Dykhuizen, R. C., Robino, C. V., & Knorovsky, G. A. (1999). A method for extracting phase change kinetics from dilatation for multistep transformations: Austenitizȧtion of a low carbon steel. *Metallurgical and Materials Transactions B: Process Metallurgy and Materials Processing Science*, *30*(1), 107–117. https://doi.org/10.1007/s11663-999-0011-z

Enomoto, M., & Hayashi, K. (2018). Modeling the growth of austenite in association with cementite during continuous heating in low-carbon martensite. *Journal of Materials Science*, *53*(9), 6911–6921. https://doi.org/10.1007/s10853-018-2020-2

Enomoto, M., & Hayashi, K. (2019). Simulation of Austenite Formation During Continuous Heating from Low Carbon Martensite with Poly-dispersed Cementite. *Metallurgical and Materials Transactions A: Physical Metallurgy and Materials Science*. https://doi.org/10.1007/s11661-019-05569-3

Eres-Castellanos, A., Garcia-Mateo, C., & Caballero, F. G. (2021). Future Trends on Displacive Stress and Strain Induced Transformations in Steels. *Metals 2021, Vol. 11, Page 299*, *11*(2), 299. https://doi.org/10.3390/MET11020299

Erisir, E., Gürkan Bilir, O., Erişir, E., & Bilir, G. (2015). *Nucleation and Growth of Austenite from Martensite during Reaustenization using Phase Field Modeling*. https://www.researchgate.net/publication/274567810

Esin, V. A., Denand, B., Le Bihan, Q., Dehmas, M., Teixeira, J., Geandier, G., Denis, S., Sourmail, T., & Aeby-Gautier, E. (2014). In situ synchrotron X-ray diffraction and dilatometric study of austenite formation in a multi-component steel: Influence of initial microstructure and heating rate. *Acta Materialia*, *80*, 118–131. https://doi.org/10.1016/j.actamat.2014.07.042

García De Andrés, C., Caballero, F. G., Capdevila, C., & Bhadeshia, H. K. D. H. (2001). *MODELLING OF KINETICS AND DILATOMETRIC BEHAVIOR OF NON-ISOTHERMAL PEARLITE-TO-AUSTENITE TRANSFORMATION IN AN EUTECTOID STEEL*.

Garcin, T., Ueda, K., & Militzer, M. (2017). Reverse Austenite Transformation and Grain Growth in a Low-Carbon Steel. *Metallurgical and Materials Transactions A: Physical Metallurgy and Materials Science*, *48*(2), 796–808. https://doi.org/10.1007/s11661-016-3855-2

Garcıa de Andrés, C., Caballero, F. G., Capdevila, C., & San Martın, D. (2002). Revealing austenite grain boundaries by thermal etching: advantages and disadvantages. *Materials Characterization*, *49*(2), 121–127.

Gaude-Fugarolas, D., & Bhadeshia, H. K. D. H. (2003). A model for austenitisation of hypoeutectoid steels. *Journal of Materials Science*, *38*(6), 1195–1201. https://doi.org/10.1023/A:1022805719924

Hamada, S., Sasaki, D., Ueda, M., & Noguchi, H. (2011). Fatigue limit evaluation considering crack initiation for lamellar pearlitic steel. *Procedia Engineering*, *10*, 1467–1472. https://doi.org/10.1016/J.PROENG.2011.04.245

Herrejón-Escutia, M., Solorio-Díaz, G., Vergara-Hernández, H. J., López-Martínez, E., & Vázquez-Gómez, O. (2019). Dilatometric model for determining the formation of austenite during continuous heating in medium carbon steel. *Journal of Thermal Analysis and Calorimetry*, *137*(2), 399–410. https://doi.org/10.1007/s10973-018-7936-x

Hunkel, M., Surm, H., & Steinbacher, M. (2018). *Dilatometry* (pp. 103–129). https://doi.org/10.1016/B978-0-444-64062-8.00019-X

Law, N. C., & Edmonds, D. V. (1980). The formation of austenite in a low-alloy steel. *Metallurgical and Materials Transactions A*, *11*(1), 33–46. https://doi.org/10.1007/BF02700436

Lévesque, J. B., Lanteigne, J., Champliaud, H., & Paquet, D. (2020). Modeling Solid-State Phase Transformations of 13Cr-4Ni Steels in Welding Heat-Affected Zone. *Metallurgical and Materials Transactions A: Physical Metallurgy and Materials Science*, *51*(3), 1208–1220. https://doi.org/10.1007/s11661-019-05587-1

Li, D., Min, Y. A., & Wu, X. C. (2010). Calculation of austenite formation kinetics of copper-bearing steel during continuous heating. In *Journal of Iron and Steel Research International* (Vol. 17, Number 11, pp. 62–66). https://doi.org/10.1016/S1006-706X(10)60171-9

Li, Z. D., Yang, Z. G., Pan, T., Xia, Z. X., & Zhang, C. (2011). Analytical modeling of austenite growth and phase evolution during reverse transformation from pearlite in high carbon steels. *Solid State Phenomena*, *172–174*, 1201–1206. https://doi.org/10.4028/www.scientific.net/SSP.172-174.1201

Li, Z., Wen, Z., Su, F., Zhang, R., & Zhou, Z. (2018). Dilatometric research on pearlite-to-austenite transformation of Fe–1C–1.44Cr low-alloy steel. *Journal of Materials Science*, *53*(2), 1424–1436. https://doi.org/10.1007/s10853-017-1556-x

Lopes, M. M. B., & Cota, A. B. (2014). A study of isochronal austenitization kinetics in a low carbon steel. *Rem: Revista Escola de Minas*, *67*(1), 61–66. https://doi.org/10.1590/s0370-44672014000100009

López-Martínez, E., Vázquez-Gómez, O., Vergara-Hernández, H. J., & Campillo, B. (2015). Effect of initial microstructure on austenite formation kinetics in high-strength experimental microalloyed steels. *International Journal of Minerals, Metallurgy and Materials*, *22*(12), 1304–1312. https://doi.org/10.1007/s12613-015-1198-4

Mattos Ferreira, V., Mecozzi, M. G., Petrov, R. H., & Sietsma, J. (2023). Details of pearlite to austenite transformation in steel: Experiments and phase-field modeling. *Computational Materials Science*, *228*, 112368. https://doi.org/10.1016/J.COMMATSCI.2023.112368

Mohsenzadeh, M. S., & Mazinani, M. (2019). The Influence of Microstructural Characteristics on Austenite Formation Kinetics in a Plain Carbon Steel. *Metallurgical and Materials Transactions A: Physical Metallurgy and Materials Science*, *51*(1), 116–130. https://doi.org/10.1007/s11661-019-05470-z

Mustak, O., Evcil, E., & Simsir, C. (2016). Simulation of through-hardening of SAE 52100 steel bearings - Part I: Determination of material properties. *MATERIALWISSENSCHAFT UND WERKSTOFFTECHNIK*, *47*(8), 735–745. https://doi.org/10.1002/MAWE.201600607

Nishiyama, Z. (2012). *Martensitic transformation*. Academic Press.

Oliveira, F. L. G., Andrade, M. S., & Cota, A. B. (2007). Kinetics of austenite formation during continuous heating in a low carbon steel. *Materials Characterization*, *58*(3), 256–261. https://doi.org/10.1016/j.matchar.2006.04.027

Paul Shewmon. (2016). *Diffusion in Solids*. Springer Cham.

Pereloma, E., & Edmonds, D. (2012). *Phase transformations in steels: Diffusionless transformations, high strength steels, modelling and advanced analytical techniques*. Woodhead Publishing.

Pontevedra, V., Alexander, V., Dmitry, S., Semen, S., & Nikolay, K. (2019). ScienceDirect ScienceDirect ScienceDirect Modeling of Austenitization Kinetics under Continuous Heating of Modeling of Austenitization Kinetics under Continuous Heating of Steels Microstructure Steels with Complex Microstructure models for capacity optimi. *Procedia Manufacturing*, *37*, 613–620. https://doi.org/10.1016/j.promfg.2019.12.096

Porter, D. A., Easterling, K. E., & Sherif, M. Y. (2021). Phase Transformations in Metals and Alloys, Fourth Edition. *Phase Transformations in Metals and Alloys, Fourth Edition*, 1–556.

Ranjan, R., & Singh, S. B. (2019). Formation of austenite in steels during heating: analysis of dilatation data. *Materials Science and Technology (United Kingdom)*, *35*(7), 782–790. https://doi.org/10.1080/02670836.2019.1591026

Reed-Hill, R., Abbaschian, R., & Abbaschian, R. (1973). *Physical metallurgy principles*. http://sutlib2.sut.ac.th/sut_contents/H132782.pdf

Rezaei, J., Habibi Parsa, M., & Mirzadeh, H. (2023). Phase transformation kinetics of high-carbon steel during continuous heating. *Journal of Materials Research and Technology*, *27*, 2524–2537. https://doi.org/10.1016/J.JMRT.2023.10.089

Roosz, A., Cacsi, Z., & Fuchs, E. G. (1982). *Isothermal Formation of Austenite in Eutectoid Plain Carbon Steel*.

Sadeghifar, M., Sedaghati, R., Jomaa, W., & Songmene, V. (2018). Finite element analysis and response surface method for multi-performance optimization of radial turning of hard 300M steel. *International Journal of Advanced Manufacturing Technology*, *94*(5–8), 2457–2474. https://doi.org/10.1007/s00170-017-1032-4

Settimi, A. G., Chukin, D., Pezzato, L., Gennari, C., Brunelli, K., & Dabalà, M. (2019). The impact of high heating rates on the austenitization process of 18NiCrMo5 steel. *Materials Physics and Mechanics*, *42*(6), 717–730. https://doi.org/10.18720/MPM.4262019_4

Shinozaki, T., Tomota, Y., Fukino, T., & Suzuki, T. (2017). Microstructure evolution during reverse transformation of austenite from tempered martensite in low alloy steel. *ISIJ International*, *57*(3), 533–539. https://doi.org/10.2355/isijinternational.ISIJINT-2016-557

Singh, J., & Wayman, C. M. (1987). *Formation of Secondary Austenite during the martensite to austenite Transformation in an Fe-Ni-Mn Alloy*. *93*, 227–233.

Speer, J. G., & Gaster, R. J. (2018). Austenitizing in Steels. *Steel Heat Treating Fundamentals and Processes*, *4*, 309–316. https://doi.org/10.31399/asm.hb.v04a.a0005786

Speich, G. R., Demarest, V. A., & Miller, R. L. (1981). *Formation of Austenite During Intercritical Annealing of Dual-Phase Steels*.

Talebi, S. H. (2018). *Microstructure evolution and optimization of the tempering heat treatment of a medium-carbon low-alloy steel*. École de technologie supérieure.

Talebi, S. H., Ghasemi Nanesa, H., Jahazi, M., & Melkonyan, H. (2018). Influence of starting microstructure on dilatation behavior during tempering of a high strength steel. *Trans Tech Publ*. https://doi.org/10.4028/www.scientific.net/MSF.941.305

Vasilyev, A. A., Sokolov, D. F., Sokolov, S. F., & Rudskoy, A. I. (2019). Investigation and modeling the austenitization kinetics of steels with complex microstructure under

continuous heating. *Materials Physics and Mechanics*, *42*(4), 423–435. https://doi.org/10.18720/MPM.4242019_7

Wang, L. M., Wang, Z. B., & Lu, K. (2011). Grain size effects on the austenitization process in a nanostructured ferritic steel. *Acta Materialia*, *59*(9), 3710–3719. https://doi.org/10.1016/j.actamat.2011.03.006

Wang, W., Wang, L., & Lyu, P. (2022). Kinetics of austenite growth and bainite transformation during reheating and cooling treatments of high strength microalloyed steel produced by sub-rapid solidification. *International Journal of Minerals, Metallurgy and Materials 2023 30:2*, *30*(2), 354–364. https://doi.org/10.1007/S12613-022-2548-7

Wei, R., Enomoto, M., Hadian, R., Zurob, H. S., & Purdy, G. R. (2013). Growth of austenite from as-quenched martensite during intercritical annealing in an Fe-0.1C-3Mn-1.5Si alloy. *Acta Materialia*, *61*(2), 697–707. https://doi.org/10.1016/j.actamat.2012.10.019

Yang, J. R. (1991). *Continuous Heating Transformation of Bainite to Austenite*. *131*, 99–113.

Yang, J. R., & Bhadeshia, H. K. D. H. (1989). Reaustenitization Experiments on some High-strength Steel Weld Deposits. In *Science and Engineering* (Vol. 8).

Yang, J. R., & Bhadeshia, H. K. D. H. (1991). *Continuous Heating Transformation of Bainite to Austenite*.

Yang, J. R., & Huang, C. Y. (1993). Formation of austenite from a mixture of bainitic ferrite and austenite. *Materials Chemistry and Physics*, *35*(2), 168–175. https://doi.org/10.1016/0254-0584(93)90194-Q